RESONANCE COMPENSATION STUDIES AT THE FNAL RECYCLER RING

By

Cristhian Gonzalez-Ortiz

A DISSERTATION

Submitted to
Michigan State University
in partial fulfillment of the requirements
for the degree of

Physics—Doctor of Philosophy

2024

ABSTRACT

ACKNOWLEDGEMENTS

Your acknowledgements here.

TABLE OF CONTENTS

LIST OF ABBREVIATIONS

MSU Michigan State University

FNAL Fermilab National Accelerator Laboratory

RR Recycler Ring

MI Main Injector

RDTs Resonance Driving Terms

NuMI Neutrinos at the Main Injector

PSB CERN Proton Synchrotron Booster

CHAPTER 1

INTRODUCTION

Particle accelerators are the workhorses for modern scientific discoveries. Experimental nuclear and particle physics research benefit greatly from the progress of accelerator physics and technology. Accelerator physics is a rich field of applied physics living on the intersection of electromagnetism, solid-state and atomic physics, nonlinear mechanics, plasma physics, quantum mechanics, just to name a few [1]. Furthermore, the design and operation of modern accelerator projects require costly enterprises of scientists, engineers, operators, and politicians coming together under one single metaphorical roof. Everyone coming together to perform “megascience” [2].

The scientific principle of particle accelerators involves the acceleration, steering and/or storage of charged particles through electromagnetic manipulations. These manipulations occur through a plethora of devices and components that can control electromagnetic fields, e.g., magnets, electrical cavities. The group of particles that is subject to this electromagnetic handling is referred to as "the beam". The field of beam dynamics studies the interaction between the beam and the steering devices, as well as the Coulomb interactions between the beam itself—this is known as space charge physics. An additional distinction can be made when these steering devices are configured in a circular or linear fashion. This gives rise to the distinction between circular accelerators and linear accelerators (Linacs).

Furthermore, particle accelerators can be categorized by the type of elementary particles that compose the beam and how close to the speed of light they are traveling. The first category refers to the distinction between hadrons and leptons—particles that interact or do not interact through the strong force, respectively [3]. For example, protons and heavy ions are considered hadrons, while electrons and muons are considered leptons. The second category can be summarized if particles in the machine travel at a high or low energy. An example of a low-energy hadron machine is the heavy ion Linac at FRIB (Facility for Rare Isotope Beams) [4]. An example of a high-energy lepton machine was the Stanford Linear Accelerator located at SLAC National Accelerator Laboratory [5]. The two most famous high-energy hadron machines in history are the Tevatron [6], which operated

at Fermilab, and the LHC (Large Hadron Collider), operating at CERN [7]. Furthermore, there are accelerator projects that encompass several categories such as the future EIC (Electron-Ion Collider) being built at Brookhaven National Laboratory [8], which will use an electron ring—a lepton machine—and a heavy-ion circular accelerator—a hadron machine—to probe new physics. This is just to name a few. There's a plethora of accelerator projects around the world that are either operational, under commissioning or being designed.

The following thesis will explore the beam dynamics of a circular machine used to store high-energy protons such as the Fermilab Recycler Ring.

1.1 Circular Accelerators and Storage Rings

As will become more apparent on Ch. 2, a particle accelerator can be thought of as a composition of accelerator-themed LEGO® bricks [9]. Each elemental LEGO® brick can be thought of as an accelerator component performing some mapping on the charged particles entering it. As it turns out, these LEGO® bricks can be assembled together circularly to give rise to circular accelerators. The assembly of these blocks in a particular shape gives rise to what is known as the lattice of the accelerator.

The acceleration part of these structures comes from elements inside the lattice that introduce some sort of electromotive force in the longitudinal direction. The most common example for these blocks are radio-frequency (rf) cavities [1], with super-conducting rf cavities also as an established technology [10]. Particles that go through these elements gain energy on every pass. For the case where there are no acceleration blocks on these structures, a storage ring arises. Nevertheless, storage rings can also have rf cavities just for longitudinal beam manipulation, but no overall acceleration—such is the case of the Recycler Ring.

Circular accelerators are special due to the fact that particles have to pass thousands or even millions of turns through the same LEGO® blocks. This gives birth to very interesting and complex dynamics inside these machines. One of these phenomena are called betatron resonances. The most simple lattice of a high energy machine is composed of focusing and steering blocks, and they are dipole and quadrupole magnets, i.e. the lowest-order multipole magnets. For reasons that

will become apparent in Ch. 2, these elements, in combination with free drift spaces, represent linear blocks. For the simplest circular machine, these linear LEGO® bricks are assembled together to create a linear lattice. A linear lattice is designed to have stable particle orbits all around the accelerator. Nevertheless, accounted or unaccounted elements, described by linear or nonlinear blocks, around the machine can perturb the stable orbits. Ultimately, the effect of these perturbations can add up coherently over many turns to push the beam out of the acceptance of the lattice. This whole process is known as a betatron resonance in a circular accelerator. A mathematical description of this process is described on Ch. 2.

The following thesis describes an effort to mitigate the deleterious effect of these resonances in the Recycler Ring. After dipole and quadrupole, the third order of multipole magnetic fields is the sextupole component. Therefore, sextupole fields around the lattice are the source of third order betatron resonances. Specifically, this thesis explores mitigation techniques to these third order resonances, mainly in the Fermilab Recycler Ring (see Ch. 3, Ch. 5 and Ch. 6), but also with some experiments done at the CERN Proton Synchrotron Booster (see Ch. 4).

1.2 Fermilab

The best introduction to Fermilab is to cite an excerpt from Ref. [2]:

> [...] A passenger peers through the window of an airplane. As his plane flies into Chicago's O'Hare Field from the west, he notices a large ring on the ground below (see Fig. 1.1). Near it he sees a towering white structure, a group of colorful smaller buildings, an expanse of forest, open fields, and lakes.
>
> "What is that ring?" he asks his neighbor.
>
> "Fermilab," she replies. "It's a physics laboratory. The government supports research there into what the universe is made of."
>
> "Why the ring?"
>
> "It's the four-mile-round main ring of a machine called the Tevatron. It turns protons into tools for looking inside the atomic nucleus. Huge magnets steer the protons

around the ring, while high voltages accelerate them. [...]" (pp. 1)

Figure 1.1 Aerial view of the Fermi National Accelerator Laboratory (FNAL) located in Batavia, IL, USA [11].

The Fermi National Accelerator Laboratory (FNAL), better known as Fermilab, has a long and rich history of designing, building and operating high-energy particle accelerators. Ever since the founding director of Fermilab, Robert R. Wilson, envisioned the 400 GeV Main Ring back in 1967, Fermilab has been at the forefront of accelerator physics [2, 6, 12]. The most famous accelerator project hosted by Fermilab has been the Tevatron, a proton-antiproton circular collider with a circumference of around 6.28 km. This machine was injected protons and antiprotons from smaller machines, that are still in operation or have been repurposed as of 2024, e.g. the Recycler Ring. The Tevatron operated up until 2011, leaving an indelible legacy in the field of high energy and accelerator physics. Nostalgia aside, Fermilab still hosts a deluge of particle physics experiments connected to its main accelerator complex.

The current layout of the Fermilab Accelerator Complex is summarized in Fig. 1.2. As of 2024, the Fermilab Accelerator Complex is composed of an H^- source that connects to a linear accelerator, accelerating the ions to an energy of 400 MeV. This linear accelerator feeds to the first circular machine—the Booster—where protons are achieved and accelerated to an energy of 8 GeV. After the Booster, the protons are transported to the Recycler Ring (RR), which is the second circular machine. In the RR, protons are stacked and stored in order to increase the beam intensity delivered to the Main Injector (MI). This last circular accelerator is where protons are accelerated from an energy of 8 GeV to 120 GeV. Once at this energy, the protons are transported the Neutrinos at the Main Injector (NuMI) experiment, in order to create the world's most intense neutrino beam [13]. Nevertheless, all throughout the chain of accelerators, beam is also delivered to a plethora of other experiments being conducted at Fermilab. Therefore, the facility has several modes of operation depending on the experiments that are online. A more detailed and technical study of the current Fermilab Accelerator Complex, focusing on the Recycler Ring, is given on Ch. 3.

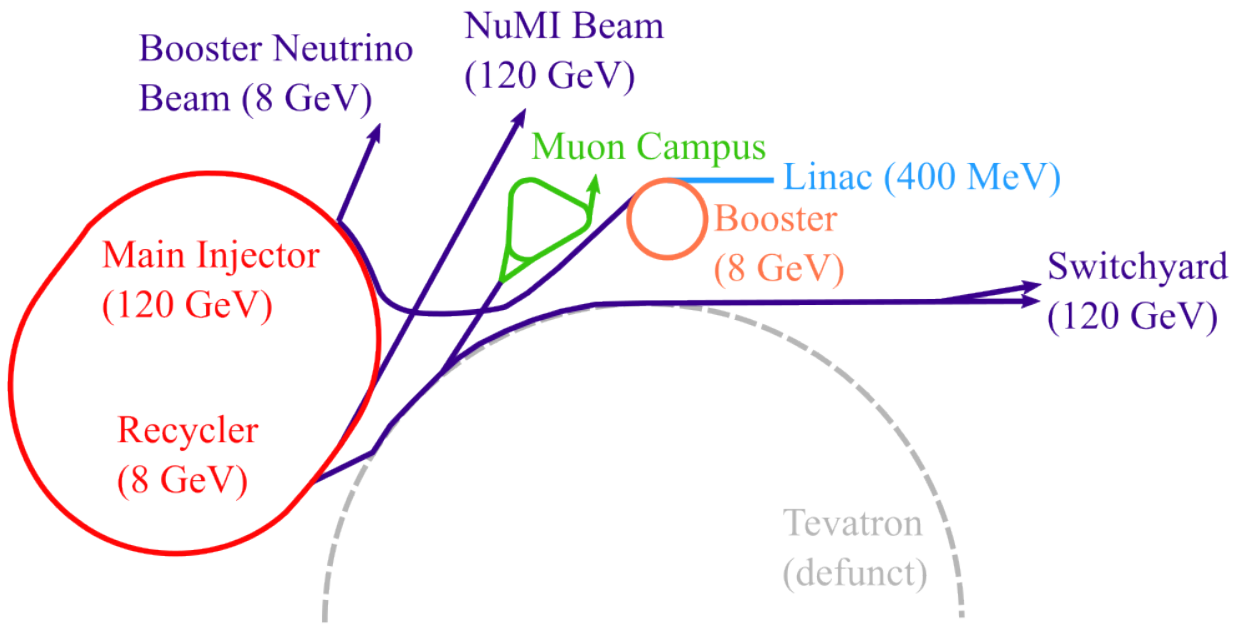

Figure 1.2 Schematic layout of the Fermilab Accelerator Complex as of 2024. Original plot provided by R. Ainsworth, first published on Ref. [14].

1.3 Outline

The following thesis will explore the compensation of third-order resonances in the Fermilab Recycler Ring. Chapter 1 introduces the motivation behind this thesis work. Chapter 2 summarizes single particle dynamics with the help of exponential Lie operators and moves forward to introduce a relevant concept of collective beam dynamics: the space charge tune shift. This theoretical overview gives segue into the Ch. 3 of this thesis, where the Recycler Ring is introduced and described in detail. Motivation for the compensation of third order resonances is given in this chapter under the framework of current and future operation of the RR. With the basic physics concepts and the description of the machine put in place, Ch. 4 describes in full detail the scheme and experiments developed in order to compensate third order resonances at low intensities. Before moving to explore the Recycler Ring at high intensities, Ch. 5 provides an interlude in order to show a series of experiments done at the CERN PS Booster. These experiments explore the use of advanced optimization algorithms in the aid of compensating multiple resonance lines simultaneously. Coming back to Fermilab, Ch. 6 showcases the studies and experiments done at high intensities in the RR in order to understand the interplay between the compensation of resonance lines and space charge effects. Finally, Ch. 7 brings down the curtain by providing some general conclusions and future work stemming from this thesis.

CHAPTER 2

BEAM DYNAMICS IN RINGS

2.1 Introductory Accelerator Physics

The basic building blocks of a particle accelerator are the elements that steer and focus the beam in the transverse direction. This is done by utilizing and manipulating the Lorentz force $\vec{F}_L$ by means of the electromagnetic fields $\vec{E}$ and $\vec{B}$ to act on some particle with charge q and velocity $\vec{v}$, i.e., $\vec{F}_L = q\left(\vec{E} + \vec{v} \times \vec{B}\right)$. While there are a handful of electromagnetic devices that can do this, the most prominent ones in high-energy accelerators are magnets which have no electric field, $\vec{E} = 0$. In particular, there are pure dipole magnets for steering and pure quadrupole magnets for focusing. Nevertheless, some machines such as the Recycler Ring have combined function magnets which can have both types of magnets—and even higher order magnets—embedded in one, in order to steer and focus the particles. The previous information assumes that every magnet can be expanded and described as a decomposition of magnetic multipoles, where dipole and quadrupole components are the lowest order terms of the expansion. Therefore, using the Beth representation [1], the multipole expansion for an arbitrary multipole magnet reads:

$$\frac{1}{[B\rho]}\left(B_y(x,y) + iB_x(x,y)\right) = -\frac{1}{\rho}\sum_{n=0}^{\infty}\left(b_n + ia_n\right)(x+iy)^n\,, \tag{2.1}$$

where b_n and a_n are the multipole coefficients defined by

$$b_n = \frac{1}{B_0 n!}\left.\frac{\partial^n B_y}{\partial x^n}\right|_{x=y=0}, \quad a_n = \frac{1}{B_0 n!}\left.\frac{\partial^n B_x}{\partial x^n}\right|_{x=y=0}. \tag{2.2}$$

For Eqs. 2.1 and 2.2, x and y represent the Cartesian coordinates, the product $[B\rho]$ represents the magnetic rigidity of the beam with B_0 being the main dipole field and ρ is the bending radius, while B_x and B_y are the transverse magnetic fields in the magnets. Specifically, the coefficients b_n and a_n represent the multipole coefficient of the magnet with the dipole coefficient defined as $b_0 = 1$, such that $B_0 b_0 = -[B\rho]/\rho$. Following the expansion, the term a_0 is referred to as the dipole roll coefficient, b_1 as the quadrupole coefficient, a_1 as the skew quadrupole coefficient, b_2 as the sextupole coefficient, a_2 for the skew sextupole coefficient, b_3 for the octupole coefficient, a_3 for the skew octupole coefficient, etc. This is all following the U.S. convention.

The most basic circular accelerator of circumference C is composed of LEGO® blocks chosen from a pile of dipoles, quadrupoles and free drift spaces. Each of these elements are described by Eqs. 2.1 and 2.2, i.e., for the quadrupole case, the only nonzero coefficient is b_1. The particles inside this ring have a longitudinal relativistic velocity of $v = \beta_L c$, and therefore have a revolution frequency of $f_{rev} = \beta_L c/C$. The Hamiltonian of a single particle with position coordinates x, y and momentum coordinates p_x, p_y traversing through such a system at an independent time coordinate s is:

$$H = \frac{1}{2}\left(K_x(s)x^2 + \frac{1}{2}K_y(s)y^2 + p_x^2 + p_y^2\right), \tag{2.3}$$

where $K_x(s), K_y(s)$ are the effective focusing functions, and are defined as:

$$K_x(s) = \frac{1}{\rho^2} - \frac{b_1(s)}{\rho}, \quad K_y(s) = \frac{b_1(s)}{\rho} \tag{2.4}$$

assuming the definition of $b_1(s)$ in 2.2 has been extended to describe the distribution of the horizontal quadrupole coefficient around the ring. For the case where $\rho \gg 1$ (high-energy limit), the function $K_y(s) = -K_x(s)$, i.e., horizontally focusing quadrupoles will have a defocusing effect in the vertical direction and vice versa.

In classic accelerator references, such as Refs. [1, 15, 16], the equations of motion derived from the Hamiltonian in Eq. 2.3 are known as Hill's equations. The usual accelerator-physics method to solve this type of equations is to introduce transfer matrices for each type of linear element. This will define linear mappings bringing some initial state vector $\vec{X}_0 = \left(x_0, x_0', y_0, y_0'\right)$ to a final vector $\vec{X}_f = \left(x_f, x_f', y_f, y_f'\right)$ using a symplectic matrix M, i.e., $\vec{X}_f = M\vec{X}_0$. Table 2.1 shows the 4D transfer matrices for common linear elements found in accelerators. It is worth noting that these 4D matrices can be used to include coupling elements that couple the $x - y$ plane. For this case, the off-block coefficients of the matrices would be non-zero. An example of this last case is shown in Table 2.1 by means of the thin skew quadrupole case. Nevertheless, the starting point of this work is to consider a circular accelerator built from linear non-coupling elements, while other coupling or nonlinear elements are considered perturbative. In Sec. 2.2, Lie operators are used in order to extend these mappings to the nonlinear regime.

Table 2.1 Transfer matrices for common accelerator elements in the high-energy regime and paraxial approximation

Element	**4D Transfer Matrix**
Drift space of length L	$M = \begin{bmatrix} 1 & L & 0 & 0 \\ 0 & 1 & 0 & 0 \\ 0 & 0 & 1 & \mathrm{L} \\ 0 & 0 & 0 & 1 \end{bmatrix}$
Dipole of bending radius ρ, length ℓ and orbiting angle $\theta = \ell/\rho$	$M = \begin{bmatrix} \cos\theta & \rho\sin\theta & 0 & 0 \\ -\frac{1}{\rho}\sin\theta & \cos\theta & 0 & 0 \\ 0 & 0 & 1 & \ell \\ 0 & 0 & 0 & 1 \end{bmatrix}$
Thin quadrupole of focal length $f = \lim_{\ell\to 0} \frac{1}{k\ell} > 0$	$M = \begin{bmatrix} 1 & 0 & 0 & 0 \\ -1/f & 1 & 0 & 0 \\ 0 & 0 & 1 & 0 \\ 0 & 0 & 1/f & 1 \end{bmatrix}$
Thick quadrupole of strength $k > 0$ and length ℓ	$M = \begin{bmatrix} \cos\sqrt{k}\ell & \frac{1}{\sqrt{k}}\sin\sqrt{k}\ell & 0 & 0 \\ -\sqrt{k}\sin\sqrt{k}\ell & \cos\sqrt{k}\ell & 0 & 0 \\ 0 & 0 & \cosh\sqrt{\lvert k\rvert}\ell & \frac{1}{\sqrt{\lvert k\rvert}}\sinh\sqrt{\lvert k\rvert}\ell \\ 0 & 0 & \sqrt{\lvert k\rvert}\sinh\sqrt{\lvert k\rvert}\ell & \cosh\sqrt{\lvert k\rvert}\ell \end{bmatrix}$
Thin skew quadrupole of focal length $f_s = \lim_{\ell\to 0} \frac{1}{k_s\ell} > 0$	$M = \begin{bmatrix} 1 & 0 & 0 & 0 \\ 0 & 1 & 1/f_s & 0 \\ 0 & 0 & 1 & 0 \\ 1/f_s & 0 & 0 & 1 \end{bmatrix}$

Just like stacking LEGO® bricks together, these transfer matrices can be stacked up in order to calculate the total mapping through a stack of elements. The total linear mapping of a consecution of accelerator elements is just the matrix multiplication of the corresponding transfer matrices, i.e.,

for a lattice with N linear blocks the total transfer matrix reads:

$$M_{Total} = M_N M_{N-1} ... M_1. \tag{2.5}$$

Taking linear lattices one step further, the Twiss parametrization can be introduced. This parametrization employs the fact that any linear element or stack of linear elements can be parametrized by the Twiss functions $\beta_u(s), \alpha_u(s)$ and $\gamma_u(s)$ and a phase advance defined as $\phi_u(s) = \int_0^s ds/\beta_u(s)$, where u stands for either the x or y plane. This results in the following transfer matrix from location $s = 0$ to an arbitrary location s:

$$M(s) = \begin{bmatrix} M_x(s) & 0_{2\times2} \\ 0_{2\times2} & M_y(s) \end{bmatrix}, \tag{2.6}$$

where M_u is a square matrix defined as:

$$M_u = \begin{bmatrix} \sqrt{\frac{\beta_u(s)}{\beta_u(0)}} \left(\cos\phi_u(s) + \alpha_u(0)\sin\phi_u(s)\right) & \sqrt{\beta_u(s)\beta_u(0)}\sin\phi_u(s) \\ \frac{\alpha_u(0)-\alpha_u(s)}{\beta_u(s)\beta_u(0)}\cos\phi_u(s) - \frac{1+\alpha_u(0)\alpha_u(s)}{\beta_u(s)\beta_u(0)}\sin\phi_u(s) & \sqrt{\frac{\beta_u(0)}{\beta_u(s)}}\left(\cos\phi_u(s) - \alpha_u(s)\sin\phi_u(s)\right) \end{bmatrix}, \tag{2.7}$$

and $0_{2\times2}$ is a square matrix of size 2×2 with zeros in all of its entries. As a consequence of the Twiss parametrization, the position coordinate at an arbitrary s along a linear lattice may be expressed as:

$$u(s) = \sqrt{2J_u\beta_u(s)}\cos\left(\phi_u(s) + \phi_{u0}\right), \tag{2.8}$$

where J_u is a constant of motion known as the action and ϕ_{u0} is an arbitrary phase constant. Equation 2.8 describes what is known as betatron oscillations. Additionally, the action J_u can be calculated as

$$2J_u = \gamma_u u^2 + 2\alpha_u u u' + \beta_u u'^2, \tag{2.9}$$

for any s using the property $\beta_u\gamma_u = 1+\alpha_u^2$. Therefore, the particles traversing through the lattice will exhibit oscillatory motion, with amplitude dictated by the $\beta_u(s)$ function and frequency dictated by the $\phi_u(s)$ function.

Up until now, all of this formalism can be applied to either a linear or circular accelerator. No assumption has been made on how the stacking of the LEGO® bricks in the lattice affects

this formalism. Nevertheless, in a circular accelerator of circumference C there is an additional constraint on the Twiss functions given that there exists periodic boundary conditions, i.e., $\beta(s) = \beta(s + C)$, and similarly for the other Twiss functions. Another important parameter for a circular lattice is the tune Q_u, defined as the total phase advance over one turn of the machine, i.e.,

$$2\pi Q_u = \phi_u(C) = \int_s^{s+C} \frac{ds}{\beta_u(s)}. \tag{2.10}$$

With the definition of the tune Q_u, Eq. 2.7 can be rewritten in order to calculate the one-turn matrix $M(C)$ of the circular accelerator, such that:

$$M(C) = \begin{bmatrix} M_x(C) & 0_{2\times2} \\ 0_{2\times2} & M_y(C) \end{bmatrix}, \tag{2.11}$$

where each plane will have its own one-turn transfer matrix reading:

$$M_u(C) = \begin{bmatrix} \cos 2\pi Q_u + \alpha_u(C) \sin 2\pi Q_u & \beta_u(C) \sin 2\pi Q_u \\ -\gamma_u(C) \sin 2\pi Q_u & \cos 2\pi Q_u - \alpha_u(C) \sin 2\pi Q_u \end{bmatrix}. \tag{2.12}$$

Ultimately, Eq. 2.12 can be used to calculate the particle's state vector after N turns, where the total transfer matrix $M_u(NC)$ will just be $M_u(NC) = M_u(C)^N$. In fact, if a particle with some initial conditions is tracked for enough turns and its geometrical coordinates (x, x, y, y') are recorded through some diagnostic device every turn, the resulting trajectory would lie on an ellipse—the phase space ellipse. The astute reader would have already identified that Eq. 2.9 hinted to this fact, given that this is just the implicit definition for an ellipse. In essence, the Twiss parametrization will give the geometry in order to fully describe the ellipse. These statements are illustrated in Fig. 2.1, where the phase space ellipse is drawn with geometrical quantities associated to the Twiss functions.

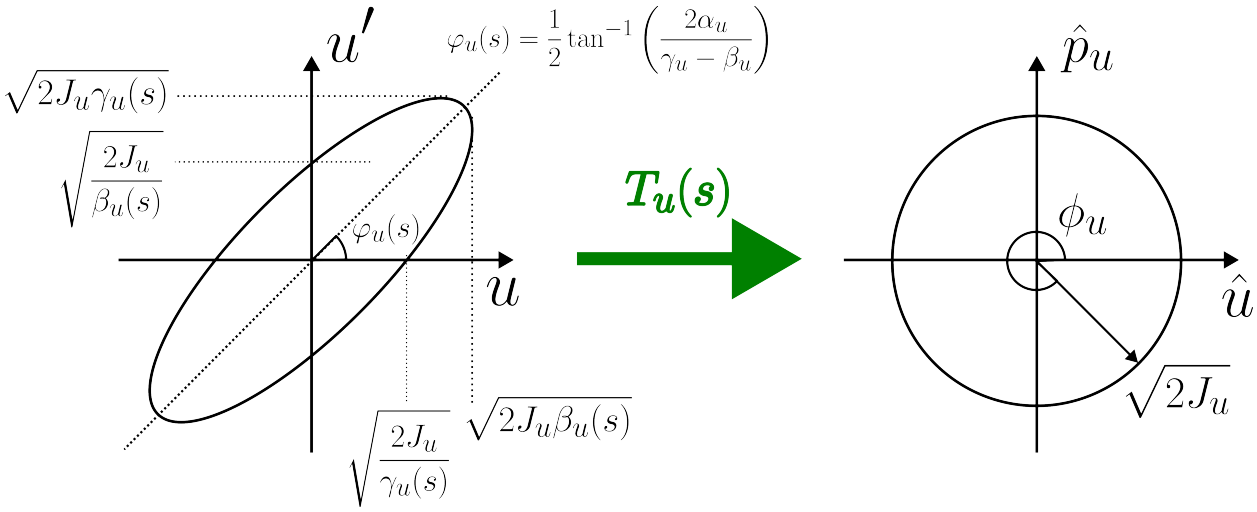

Figure 2.1 Phase space ellipse in geometrical coordinates with Twiss parametrization and its counterpart transformation in normalized phase space.

Figure 2.1 also hints at the fact that a linear transformation $T_u(s)$ can be done in order to transform the phase space ellipse into a circle. This is referred to as a Floquet transformation. Therefore, a change of coordinates from geometrical coordinates (u, u') to normalized coordinates $(\hat{u}, \hat{p}_u)$ can be achieved through the following linear transformation:

$$\begin{bmatrix} \hat{u} \\ \hat{p}_u \end{bmatrix} = \begin{bmatrix} \frac{1}{\sqrt{\beta_u}} & 0 \\ \frac{\alpha_u}{\beta_u} & \sqrt{\beta_u} \end{bmatrix} \begin{bmatrix} u \\ u' \end{bmatrix} = \sqrt{2J_u} \begin{bmatrix} \cos\phi_u(s) \\ -\sin\phi_u(s) \end{bmatrix}. \tag{2.13}$$

Ultimately, Floquet and his transformations show that the one-turn Hamiltonian for circular accelerators can be expressed as:

$$H_0 = 2\pi Q_x J_x + 2\pi Q_y J_y, \tag{2.14}$$

which is simpler and more succinct than the Hamiltonian in Eq. 2.3. Conclusively, all the dynamics of a linear circular accelerator with all of its intricacies can be mapped to rotations on a simple circle. The dynamics in normalized phase space is just parametrized by a rotation matrix $R(s)$, that will depend on the lattice itself, and is analogous to the transfer matrices $M(s)$ in geometrical space. Therefore, linear dynamics in a circular accelerator can be summarized with the following

commutative diagram:

$$\begin{array}{ccc} \begin{pmatrix} x, x' \\ y, y' \end{pmatrix}_0 & \xrightarrow{M(s)} & \begin{pmatrix} x, x' \\ y, y' \end{pmatrix}_f \\ \Big\downarrow T(s) & & \Big\downarrow T(s) \\ \begin{pmatrix} J_x, \phi_x \\ J_y, \phi_y \end{pmatrix}_0 & \xrightarrow{R(s)} & \begin{pmatrix} J_x, \phi_x \\ J_y, \phi_y \end{pmatrix}_f \end{array} . \tag{2.15}$$

Before proceeding to the next sections, where Lie operators are introduced in order to generalize to non-linear mappings, a short summary is adequate. For a linear circular accelerator, the last section has shown that starting from Hill's equation, linear transformations can be applied to a complex machine such as an accelerator in order to end up with a simple mathematical equation such as the one described in Eq. 2.14. Simply put, nonlinear elements will distort the phase space circle of Fig. 2.1, destroying the linearity of the system. The premise here is that non-linear elements in circular accelerators are inevitable, and they will come from anywhere and everywhere in the lattice, either from accounted or unaccounted sources. Therefore, higher-tier mathematical tools have to be used in order to describe non-linear dynamics in a circular accelerator. Linear matrices will only get you so far.

2.2 Lie Maps in Accelerator Physics

The most basic element of a particle accelerator can be thought of as a LEGO® brick acting as a black box transformation for a single particle. This black box takes some single charged particle with initial transverse coordinates $\left(x_0, x_0', y_0, y_0'\right)$, as defined in a Frenet-Serret coordinate system, and maps them to some final coordinates $\left(x_f, x_f', y_f, y_f'\right)$. For simplicity, any longitudinal effect will not be taken into account for this analysis, but can be easily incorporated. By gathering the initial coordinates into a vector, i.e. $\vec{X}_0 = \left(x_0, x_0', y_0, y_0'\right)$, and doing the same for the final coordinates, i.e., $\vec{X}_f = \left(x_f, x_f', y_f, y_f'\right)$, one can define the mapping $\mathcal{M}$ that relates both vectors,

such that:

$$\vec{X}_f = \mathcal{M}\vec{X}_0. \tag{2.16}$$

Different from the previous section, $\mathcal{M}$ need not be a linear mapping. For a charged particle inside some accelerator element that can be described using Hamiltonian dynamics, the mapping $\mathcal{M}$ can be understood in terms of Poisson brackets and exponential Lie operators [9, 15, 17–19].

Let $\vec{X} = (q_1, p_1, \ldots, q_n, p_n)$ be a 2n dimensional vector, made from n pairs of canonical coordinates (q_i, p_i) that make up the $2n$ dimensional phase space. And let two arbitrary functions $f\left(\vec{X}; s\right)$ and $g\left(\vec{X}; s\right)$ be functions of $\vec{X}$ and s, where s plays the role of the independent "time" coordinate. The Poisson brackets $[\bullet, \bullet]$ can be defined as:

$$[f, g] = \sum_{i=1}^{n} \frac{\partial f}{\partial q_i}\frac{\partial g}{\partial p_i} - \frac{\partial f}{\partial p_i}\frac{\partial g}{\partial q_i}. \tag{2.17}$$

Using this definition, one can explicitly write out the Poisson bracket definition for a 4 dimensional phase space described by state vector $\vec{X} = (x, x', y, y')$. This reads:

$$[f, g] = \frac{\partial f}{\partial x}\frac{\partial g}{\partial x'} - \frac{\partial f}{\partial x'}\frac{\partial g}{\partial x} + \frac{\partial f}{\partial y}\frac{\partial g}{\partial y'} - \frac{\partial f}{\partial y'}\frac{\partial g}{\partial y}. \tag{2.18}$$

The Lie operator $: f :$ acts on some function g and is the adjoint operator of the Poisson bracket operator. Its definition reads:

$$: f : g = [f, g]\,. \tag{2.19}$$

This specific $: \bullet :$ notation allows for a compact notation in order to define the exponential Lie operator. The exponential Lie operator of an arbitrary function f is defined as

$$e^{:f:}\bullet = \sum_{k=0}^{\infty} \frac{1}{k!} (: f :)^k \bullet\,. \tag{2.20}$$

For a Hamiltonian system, the mapping of coordinates from $\vec{X}_0$ to $\vec{X}_f$ follows the expression:

$$\vec{X}_f = e^{-\ell:H:}\vec{X}\Big|_{\vec{X}=\vec{X}_0}, \tag{2.21}$$

which is known as a Lie Map [17]. In this case, ℓ corresponds to the integration length of the independent coordinate. For example, for a particle traversing a magnet which has length L, the

integration length is $\ell = L$. When looking at the one-turn map, the integration length corresponds to the circumference C of the accelerator over an effective Hamiltonian H_{eff}. Furthermore, if working with action-angle variables, the integration length ℓ would just be the phase advance μ. An implementation of exponential Lie operators using *Mathematica* [20] in order to calculate 2D and 4D mappings is presented in Appendix A and in Appendix B, respectively.

2.3 One-turn Map and Normal Form

Such as LEGO® bricks can be put together to create complex structures, accelerator elements can be assembled together to create complex ring-shaped structures such as circular accelerators. In such structures, particles will experience the same one-turn mapping over thousands or even millions of turns. The one-turn map $\mathcal{M}_1$ of a circular accelerator is the composition ($\circ$) of mappings from every LEGO® element in the ring. Choosing an arbitrary initial point at $s = 0$ and going around the ring, the one-turn map describes the transformation of coordinates after one turn, i.e., $\vec{X}_{N=1} = \mathcal{M}_1 \vec{X}_0$. This map composition reads:

$$\mathcal{M}_1 = M_{N+1} \circ e^{:h_N:} \circ \cdots \circ e^{:h_2:} \circ M_2 \circ e^{:h_1:} \circ M_1 = M_{N+1} e^{:h_N:} \ldots e^{:h_2:} M_2 e^{:h_1:} M_1, \qquad (2.22)$$

where M_i is the matrix representation of a linear mapping, that does not couple $x - y$ plane, e.g., drift space mapping, quadrupole mapping. On the other hand, the map $e^{:h_i:}$ represents any linear or non-linear mapping that can be found around the machine and can be considered a perturbation to the ideal lattice including coupling elements, e.g., skew quadrupoles, higher order multipole elements. Figure 2.2 illustrates the procedure to build the one-turn map for a circular accelerator.

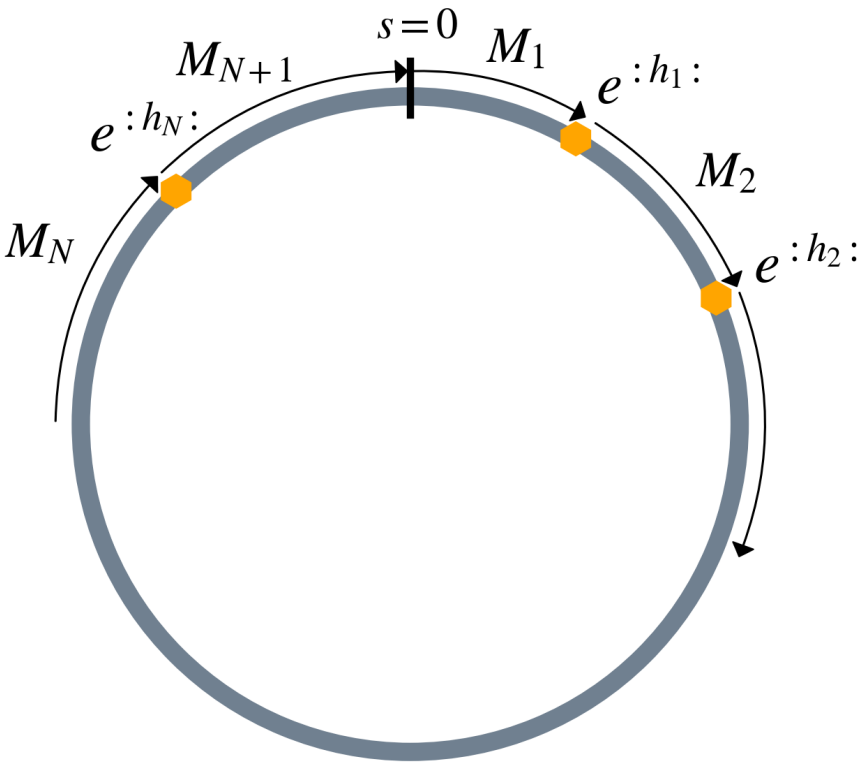

Figure 2.2 Diagram of an arbitrary circular accelerator in order to illustrate the one-turn map.

Through the use of the Baker-Campbell-Hausdorff formula [21], Eq. 2.22 can be collapsed to the expression

$$\mathcal{M}_1 = e^{-C:H_{eff}:}, \tag{2.23}$$

where C is the circumference of the ring and H_{eff} is the effective Hamiltonian of the machine over one turn. As mentioned earlier, for most cases, it is of interest to look at the perturbations to the linear uncoupled dynamics of the design lattice. With this in mind, Eq. 2.23 can be rewritten as:

$$\mathcal{M}_1 = e^{:h:}R, \tag{2.24}$$

where R is a rotation matrix encoding the linear uncoupled dynamics of the ideal lattice. On the other hand, the term $e^{:h:}$ encodes the perturbations to this ideal situation. It is worth pointing out that for the case $h = 0$, the traditional Courant-Snyder variables are recovered.

The Courant-Snyder variables $(\hat{x},\hat{p}_x,\hat{y},\hat{p}_y)$ or normalized phase space coordinates can be written for a linear uncoupled case as:

$$\hat{u} = \sqrt{2J_u}\cos\left(\phi_u + \phi_{u_0}\right); \tag{2.25}$$

$$\hat{p}_u = -\sqrt{2J_u}\sin\left(\phi_u + \phi_{u_0}\right), \tag{2.26}$$

where u can stand either for the x or y coordinate, J_u and ϕ_u correspond to the action-angle variables and ϕ_{u_0} corresponds to the initial phase. For the case where perturbations exist, i.e., $h \neq 0$, the action J_u is not constant anymore and will be a function of ϕ_u.

The Normal Form formalism is introduced at this point in order to find action-angle coordinates I_u and ψ_u, such that the motion just depends on ψ_u at a constant I_u, with some initial phase ψ_{u_0}. These are known as non-linear action-angle variables. The variables I_u and ψ_u are calculated from the transformation $e^{-:F:}$ acting on J_u and ϕ_u. The whole point is to find these variables that allow for the Hamiltonian to be only amplitude dependent. These Normal Form gymnastics can be summarized by the following commutative diagram:

$$\begin{array}{ccc} \begin{pmatrix} J_x, \phi_x \\ J_y, \phi_y \end{pmatrix}_0 & \xrightarrow{e^{:h(J_u,\phi_u):}R} & \begin{pmatrix} J_x, \phi_x \\ J_y, \phi_y \end{pmatrix}_f \\ \Big\downarrow{\scriptstyle e^{-:F:}} & & \Big\downarrow{\scriptstyle e^{-:F:}} \\ \begin{pmatrix} I_x, \psi_x \\ I_y, \psi_y \end{pmatrix}_0 & \xrightarrow[e^{:H(I_u):}]{} & \begin{pmatrix} I_x, \psi_x \\ I_y, \psi_y \end{pmatrix}_f \end{array}. \tag{2.27}$$

Without loss of generality, the generating function F can be written as a Fourier expansion over the objective space $(I_x, \psi_x, I_y, \psi_y)$ such that:

$$F = \sum_{jklm} f_{jklm} \left(2I_x\right)^{\frac{j+k}{2}} \left(2I_y\right)^{\frac{l+m}{2}} e^{i\left[(j-k)(\psi_x+\psi_{x0})+(l-m)\left(\psi_y+\psi_{y0}\right)\right]}. \tag{2.28}$$

Similarly, the argument of the Lie operator $e^{:h:}$ from Eq. 2.24 can be expanded as:

$$h = \sum_{jklm} h_{jklm} \left(2J_x\right)^{\frac{j+k}{2}} \left(2J_y\right)^{\frac{l+m}{2}} e^{i\left[(j-k)(\phi_x+\phi_{x0})+(l-m)\left(\phi_y+\phi_{y0}\right)\right]}. \tag{2.29}$$

For Eqs. 2.28 and 2.29, the integer indices j, k, l, m run from 0 to infinity, and correspond to the four degrees of freedom for transverse phase space.

The terms f_{jklm} are known as generating function coefficients. The terms h_{jklm} are known as Hamiltonian coefficients or resonance driving terms (RDTs). Section 2.5 will take a closer look into how RDTs can be used to characterize the non-linear dynamics of accelerators. The generating function coefficients f_{jklm} can be related to the Hamiltonian resonance driving terms h_{jklm} through the following relation [18, 22]:

$$f_{jklm} = \frac{h_{jklm}}{1 - e^{2\pi i\left[(j-k)Q_x + (l-m)Q_y\right]}}, \tag{2.30}$$

where Q_x and Q_y represent the transverse uncoupled and unperturbed tunes of the accelerator. The transverse tunes of a circular accelerator are defined as the phase advances in each plane over one turn, in units of 2π, i.e., $Q_u = \phi_u(s = C)/2\pi$.

In general, the terms h_{jklm} are defined by the order in which they enter the one-turn normal form Hamiltonian [22]. The general expression to define RDTs reads:

$$h_{jklm} = \Xi_{jklm} \sum_i L_i K_{n-1,i} \beta_{x,i}^{\frac{j+k}{2}} \beta_{y,i}^{\frac{l+m}{2}} e^{i\left[(j-k)\phi_{x,i} + (l-m)\phi_{y,i}\right]}, \tag{2.31}$$

where Ξ_{jklm} is just a constant defined as:

$$\Xi_{jklm} = -\frac{1}{2^n}\frac{1}{n!}\binom{n}{l+m}\binom{j+k}{j}\binom{l+m}{l}. \tag{2.32}$$

For Eqs. 2.31 and 2.32, $n = j + k + l + m$ represents the order of the RDT. The sum over i is done over all multipoles of order n and length L_i that either have a normal component $K_{n-1,i} = b_{n-1,i}/\rho$ if $l + m$ is even, or a skew component $K_{n-1,i} = a_{n-1,i}/\rho$ if $l + m$ is odd, remembering ρ is the bending radius as it appeared on Eq. 2.1. The notation $K_{n-1,i}$ is to keep up with the MAD-X convention for naming normal multipole coefficients [23]. The symbols for $\beta_{x,i}$, $\beta_{y,i}$, $\phi_{x,i}$ and $\phi_{y,i}$ represent the unperturbed beta functions and phase advances in each plane, respectively.

2.4 Resonances in Circular Accelerators

Equation 2.30 diverges for when the denominator goes to zero. Specifically, this happens when the following condition is met:

$$(j - k)\, Q_x + (l - m)\, Q_y = p, \tag{2.33}$$

where p can be any integer. Equation 2.33 defines resonance lines in tune space of order $n = j + k + l + m$. If the accelerator is tuned to operate on top of these resonances, the perturbations will add up coherently turn to turn and kick the resonant particles out of their original trajectory. In general, operating close or on top of a resonance line is harmful as particles will be lost. This is specially true for lower order resonances, i.e., for $n < 4$. In general, the higher order of a resonance, the weaker it is [16]. This thesis work focuses on third order resonances, i.e., $n = 3$, and how to mitigate their deleterious effect.

Figure 2.3 shows the tune diagram with resonance lines, as defined by Eq. 2.33, drawn up to fifth order. The integer part of both tunes are chosen to include the actual area of operation of the Recycler Ring. Nevertheless, only the fractional part of the tune carries the significant information for resonance diagrams. The operation and tune diagram for the Recycler Ring are described in more detail in Ch. 3. Normally, the operation point of a circular accelerator is chosen to be clear of any resonance line and far away as possible from integer ($n = 1$) and half integer ($n = 2$) resonances. Nevertheless, in reality there are two concepts that complicate things. The first one relates to the fact that resonance lines are not infinitely thin and have some stop bandwidth. The second one, concerns the fact that at high intensities particles will not have localized tunes, but rather a distribution of tunes with some tune spread, i.e., a tune footprint. Section 2.7 takes a closer look at this effect known as space charge tune shift. Ultimately, choosing the operation point on Fig. 2.3 is a matter of localizing a resonance-free region where the intensity-dependent tune footprint can be placed.

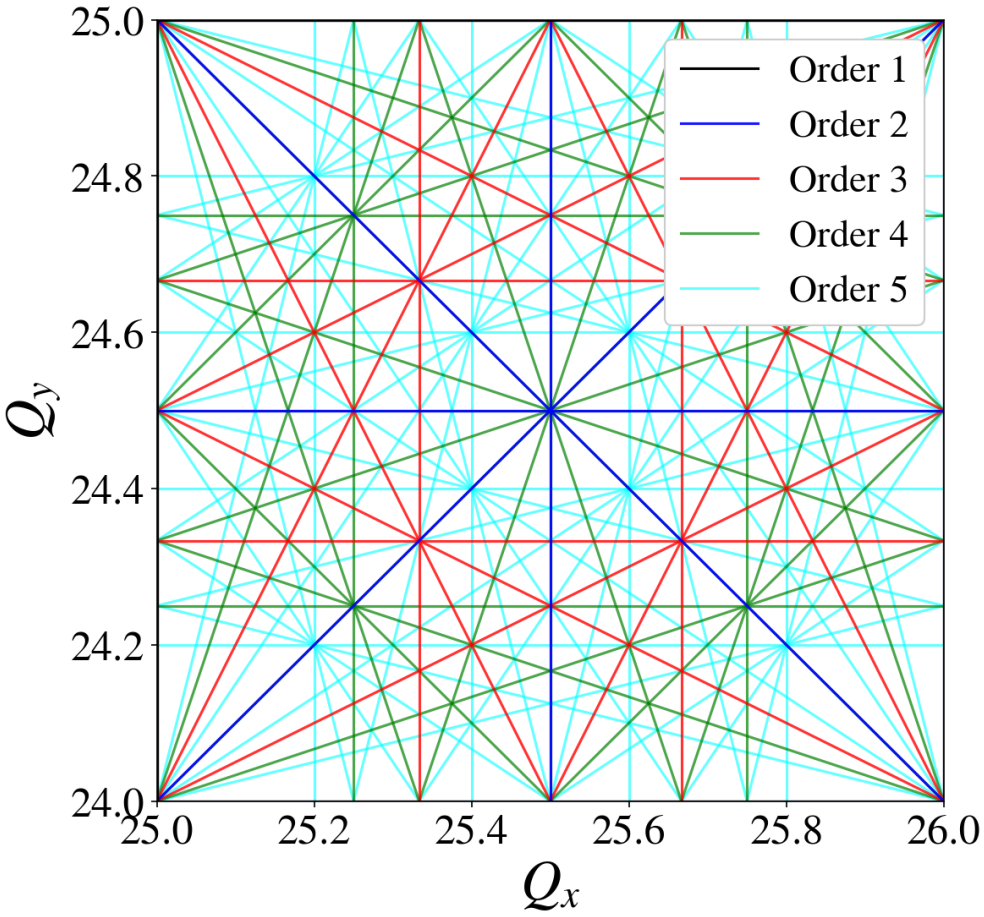

Figure 2.3 Tune diagram with resonance lines up to fifth order, enclosing the operation point of the Recycler Ring.

It is worth stopping here and asking what is the driving force behind each of these resonance lines. Classic accelerator references such as Refs. [1, 15, 16] will derive Eq. 2.33 by perturbing Hill's equation with different magnetic multipole orders. A closer look into each perturbation term reveals that half integer resonances are caused by quadrupole terms, third order resonances by sextupole-like terms, fourth order resonances by octupole terms, and so on and so forth. Nevertheless, the story complicates when one takes into account that pure multipole magnets can feed down to higher order terms, e.g., a tilted quadrupole feeds down to sextupole-like terms.

Figure 2.4 zooms into the region of interest for the Recycler Ring operation in the tune diagram, as shown in Fig. 2.3. As mentioned before, the operation point of an accelerator in the tune diagram is not a singular point but rather a footprint. While the lattice can be tuned to a specific nominal

point, particles will interact with other particles through the Coulomb force. Consequently, each particle will feel a different tune shift depending on their position within the bunch of particles. This is called the incoherent space charge tune shift, and it will be the largest for particles in the core of the bunch, i.e., the beam core. At low particle intensities, such as the one used to produce Fig. 2.4, the tune spread of the particles in the bunch is small enough to approximate the physics to single-particle dynamics. For beams with low particle intensities and a small tune spread, such as the one depicted in Fig. 2.4, operating clear from any low order resonance lines is not generally a problem. Nevertheless, at high intensities the situation changes.

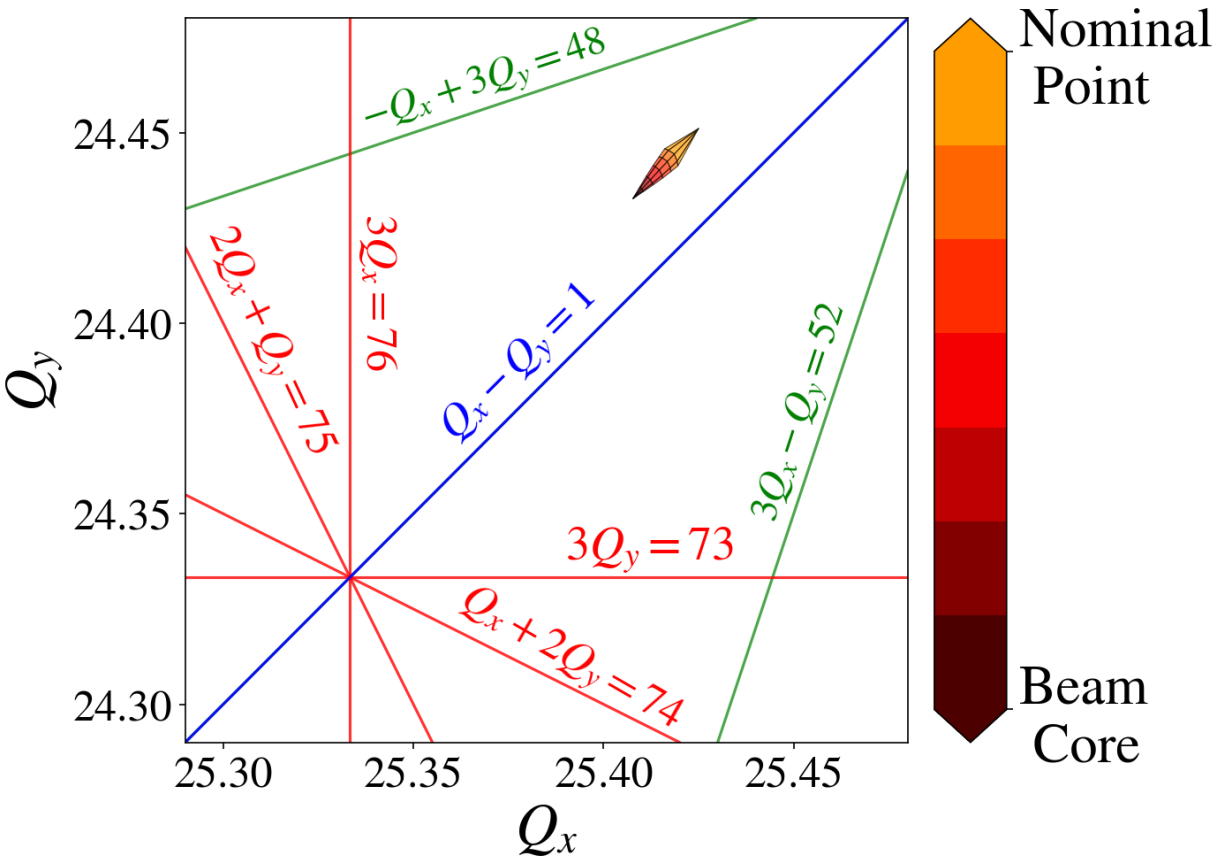

Figure 2.4 Approximate operational tune footprint at low intensities, i.e., 1e10 particles per bunch.

Figure 2.4 plots all resonance lines up to fourth order in this region of interest. The half integer line $Q_x - Q_y = 1$, also known as a difference coupling resonance, is usually driven by solenoidal and skew-quadrupole fields in the lattice. The third order lines $3Q_x = 76$ and $Q_x + 2Q_y = 74$ are

driven by sextupole-like fields. The other third order lines $3Q_y = 73$ and $2Q_x + Q_y = 75$ are driven by skew sextupole terms in the lattice. And finally, the fourth order lines $-Q_x + 3Q_y = 48$ and $3Q_x - Q_y = 52$ are driven by octupole terms in the lattice and Coulomb (space charge) forces from the bunch itself. This is assuming a rectangular multipole expansion notation of the magnetic field, such as the one presented in Eq. 2.1.

2.5 Resonance Driving Terms

The RDTs h_{jklm} are related to the strength of the resonance $(j-k)\,Q_x + (l-m)\,Q_y$. Therefore, controlling and measuring these RDTs is of special interest to accelerator physics. The following section explains how to get to a useful expression that can be used in order to measure the h_{jklm} terms through Fourier expansions.

The whole point of introducing the Normal Form coordinates (I_u, ψ_u) through the transformation $e^{-:F:}$ as defined in Eq. 2.28 is to transfer complicated non-linear dynamics to simple dynamics that lie on a circle where the action is conserved I_u and $\dot{\psi_u}$ is constant. When this happens, a set of canonical coordinates $\vec{\zeta} = \left(\zeta_x^+, \zeta_x^-, \zeta_y^+, \zeta_y^-\right)$ can be defined as:

$$\zeta_u^{\pm} = \sqrt{2I_u} e^{\mp i\left(\psi_u + \psi_{u_0}\right)}, \tag{2.34}$$

always keeping in mind that I_u is a constant of motion and ψ_{u_0} is a constant initial phase set by the initial conditions. It can be shown that the Poisson brackets for a pair of these quantities are:

$$\left[\zeta_u^+, \zeta_u^-\right]_{\psi_u, J_u} = \frac{\partial \zeta_u^+}{\partial \psi_u}\frac{\partial \zeta_u^-}{\partial J_u} - \frac{\partial \zeta_u^+}{\partial J_u}\frac{\partial \zeta_u^-}{\partial \psi_u} = -2i, \tag{2.35}$$

for the same plane u and using a reduced form of Eq. 2.18. In this notation, the subindices from $[\bullet, \bullet]_{\psi_u, J_u}$ refer to the variables to be used in order to calculate the Poisson brackets. Using Eq. 2.35, the following useful property can be derived:

$$\left[\zeta_x^{+j}\zeta_x^{-k}\zeta_y^{+l}\zeta_y^{-m}, \zeta_x^-\right]_{\psi_x, J_x} = \left(\zeta_y^{+l}\zeta_y^{-m}\right)\left[\zeta_x^{+j}\zeta_x^{-k}, \zeta_x^-\right]_{\psi_x, J_x} = -2ij\zeta_x^{+j-1}\zeta_x^{-k}\zeta_y^{+l}\zeta_y^{-m}, \tag{2.36}$$

where the last step can be achieved using Leibnitz rule for Poisson brackets, i.e., $[fg, h] = [f, h]g + f[g, h]$.

On the other hand, going back to the Courant-Snyder phase space, a set of coordinates known as a resonance basis $\vec{h} = \left(h_x^+, h_x^-, h_y^+, h_y^-\right)$ can be defined. Similarly to Eq. 2.34, the resonance basis reads:

$$h_u^{\pm} = \hat{u} \pm \hat{p_u} = \sqrt{2J_u} e^{\mp i\left(\phi_u + \phi_{u_0}\right)}, \tag{2.37}$$

always keeping in mind that in the Courant-Snyder phase space, the action J_u is a function of the phase ϕ_u, i.e., $J_u = J_u(\phi_u)$ and is not constant. The initial phase ϕ_{u_0} is again a constant set by the initial conditions.

The basis grouped in $\vec{h}$ and the one grouped in $\vec{\zeta}$ are related by the transformation:

$$\vec{h} = e^{:F\left(\vec{\zeta}\right):} \vec{\zeta}, \tag{2.38}$$

where $F(\vec{\zeta})$ is the generating function written in terms of the basis $\vec{\zeta}$. The inverse transformation to Eq. 2.38 reads:

$$\vec{\zeta} = e^{-:F\left(\vec{\zeta}\right):} \vec{h}. \tag{2.39}$$

Writing out the generating function $F(\vec{\zeta})$ in a general polynomial form, this functions reads:

$$F\left(\vec{\zeta}\right) = \sum_{jklm} f_{jklm} \zeta_x^{+j} \zeta_x^{-k} \zeta_y^{+l} \zeta_y^{-m}. \tag{2.40}$$

By inserting the definitions in Eq. 2.34 into Eq. 2.40, the proposed definition in Eq. 2.28 can be recovered.

Expanding Eq. 2.38 by using the exponential Lie operator definition from Eq. 2.20 reads:

$$\vec{h} = \vec{\zeta} + \left[F\left(\vec{\zeta}\right), \vec{\zeta}\right] + \frac{1}{2}\left[F\left[F, \vec{\zeta}\right]\right] + \ldots, \tag{2.41}$$

where this expression was truncated to second order in the Poisson brackets. By taking only the first two terms of the expansion, and introducing the expression from Eq. 2.40, one can find an approximated expression for h_x^- which reads:

$$h_x^- \approx \zeta_x^- + \left[F\left(\vec{\zeta}\right), \zeta_x^-\right] = \zeta_x^- + \sum_{jklm} f_{jklm}\left[\zeta_x^{+j} \zeta_x^{-k} \zeta_y^{+l} \zeta_y^{-m}, \zeta_x^-\right], \tag{2.42}$$

At this point is where the usefulness of Eq. 2.36 comes into play. Introducing the explicit result from Eq. 2.36 into Eq. 2.42 yields the following expression:

$$h_x^- \approx \zeta_x^- - 2i \sum_{jklm} j f_{jklm} \zeta_x^{+j-1} \zeta_x^{-k} \zeta_y^{+l} \zeta_y^{-m}. \tag{2.43}$$

Manipulating this expression further, the definition for ζ_u as described in Eq. 2.34 can be introduced into Eq. 2.43. This yields:

$$\begin{aligned} h_x^-(N) = &\sqrt{2I_x} e^{i\left(\psi_x + \psi_{x_0}\right)} \\ &- 2i \sum_{jklm} j f_{jklm} \left(2I_x\right)^{\frac{j+k-1}{2}} \left(2I_y\right)^{\frac{l+m}{2}} e^{i\left[(1-j+k)\left(\psi_x+\psi_{x_0}\right)+(m-l)\left(\psi_y+\psi_{y_0}\right)\right]}. \end{aligned} \tag{2.44}$$

At this point, Eq. 2.44 is starting to look as a useful Fourier expansion. Ultimately, the data that can be extracted from a circular accelerator will come from a diagnostic device triggered every turn, i.e., turn-by-turn data. For that reason, it will be useful to rewrite Eq. 2.44 in terms of the N number of turns of particles in the accelerator. The expression relating the phase advances to the turn number reads:

$$\psi_u = 2\pi Q_u N, \tag{2.45}$$

where $2\pi Q_u$ is the respective phase advance over one turn of the accelerator, i.e. the tune of the circular accelerator.

Therefore, the resonance basis can be built by getting the quantity $h_u^{\pm} = \hat{u} \pm \hat{p}_u$ in terms of the number of turns N and using Eq. 2.45. Specifically, for h_x^- this reads:

$$\begin{aligned} h_x^-(N) = &\sqrt{2I_x} e^{i\left(2\pi Q_x N + \psi_{x_0}\right)} \\ &- 2i \sum_{jklm} j f_{jklm} \left(2I_x\right)^{\frac{j+k-1}{2}} \left(2I_y\right)^{\frac{l+m}{2}} e^{i\left[(1-j+k)\left(2\pi Q_x N+\psi_{x_0}\right)+(m-l)\left(2\pi Q_y N+\psi_{y_0}\right)\right]}, \end{aligned} \tag{2.46}$$

where Q_x and Q_y are the horizontal and vertical uncoupled tune. Note that this analysis can be easily extended to calculate the other elements in $\vec{h}$. These calculations are left as an exercise for the reader.

2.6 Amplitude-Dependent Tune Shift

The RDT formalism allows to calculate an important quantity in accelerator physics called the amplitude-dependent tune shift. The Hamiltonian for a single particle in a linear circular lattice with perturbation elements reads:

$$H(x, y, s) = H_0(J_x, J_y) + H_1(J_x, \phi_x, J_y, \phi_y, s), \tag{2.47}$$

where H_0 is the unperturbed linear Hamiltonian with tunes Q_x and Q_y, and H_1 is the perturbation Hamiltonian stemming from linear and non-linear unaccounted blocks in the lattice.

From Secs. 2.1 and 2.3, the expressions for H_0 and H_1 have been explicitly written in Eqs. 2.14 and 2.29 in terms of J_x, ϕ_x, J_y, ϕ_y, therefore the sum of both expression reads:

$$H_0 + H_1 = 2\pi Q_x J_x + 2\pi Q_y J_y + \sum_{jklm} h_{jklm} \left(2J_x\right)^{\frac{j+k}{2}} \left(2J_y\right)^{\frac{l+m}{2}} e^{i\left[(j-k)(\phi_x+\phi_{x0})+(l-m)\left(\phi_y+\phi_{y0}\right)\right]}. \tag{2.48}$$

Nevertheless, it is important to remember that H_1 is the compilation of all perturbations after one turn to the linear Hamiltonian H_0, and is therefore perturbative.

Therefore, for Eq. 2.48, the independent time variable is the number of turns N. For this case, the equations of motion taking N as the number of turns around the circular accelerator are just:

$$\frac{\partial J_u}{\partial N} = -\frac{\partial H}{\partial \phi_u} = -\frac{\partial H_1}{\partial \phi_u}, \tag{2.49}$$

and

$$\frac{\partial \phi_u}{\partial N} = \frac{\partial H}{\partial J_u} = 2\pi Q_u + \frac{\partial H_1}{\partial J_u}. \tag{2.50}$$

This last term $\partial H_1/\partial J_u$ in Eq. 2.50 will define the amplitude-dependent tune shift. If the whole lattice were just a linear lattice, the betatron oscillations would just gain a phase change of $2\pi Q_u$ every turn, i.e., $\Delta\phi(N) = 2\pi Q_u N$. Nevertheless, given that this new term H_1 perturbs the dynamics in the accelerator, the phase change will now depend on the amplitude J_u of the betatron oscillations of the single particle. Therefore, given that this effect acts on each individual particle, it is an incoherent effect. The effective result from this new term is to detune the circular lattice from its original tune Q_u for each individual particle.

Explicitly calculating the expression from Eq. 2.50 for J_x and ϕ_x using the Hamiltonian in Eq. 2.47 yields

$$\frac{\partial \phi_x}{\partial N} = 2\pi Q_x + \sum_{jklm} h_{jklm} \left(\frac{j+k}{2}\right) (2J_x)^{\frac{j+k}{2}-1} \left(2J_y\right)^{\frac{l+m}{2}} e^{i\left[(j-k)(\phi_x+\phi_{x0})+(l-m)\left(\phi_y+\phi_{y0}\right)\right]}. \quad (2.51)$$

In particular, it is of interest to look at the average limit where particles have undergone large number of turns around the circular accelerator $N \to \infty$. This is done in order to wash out any oscillatory behavior in $\partial H_1/\partial J_u$. Therefore, the following quantity is of interest:

$$\lim_{N\to\infty} \left\langle \frac{\partial \phi_x}{\partial N} \right\rangle_N = \lim_{N\to\infty} \frac{1}{N} \int_0^N dN' \, \frac{\partial \phi_x}{\partial N'}, \quad (2.52)$$

which is just the definition for the average of $\partial\phi_x/\partial N$ over N turns, for many turns. Explicitly calculating this quantity gives:

$$\lim_{N\to\infty} \left\langle \frac{\partial \phi_x}{\partial N} \right\rangle_N = 2\pi Q_x + \sum_{jklm} h_{jklm} \left(\frac{j+k}{2}\right) \lim_{N\to\infty} \frac{1}{N} \int_0^N dN' \; (2J_x)^{\frac{j+k}{2}-1} \left(2J_y\right)^{\frac{l+m}{2}} e^{i\left[(j-k)(\phi_x+\phi_{x0})+(l-m)\left(\phi_y+\phi_{y0}\right)\right]}. \quad (2.53)$$

In general, it is known that J_u, ϕ_u depend on the number of turns, i.e., $J_u, \phi_u = J_u(N), \phi_u(N)$. Nevertheless, Eq. 2.53 can be approximated by inserting the unperturbed solution of H_0 which means that J_u is constant and $\phi_u = 2\pi Q_u N$. With this in mind and assuming the constants $\phi_{u0} = 0$ without loss of generality, Eq. 2.53 reduces to

$$\lim_{N\to\infty} \left\langle \frac{\partial \phi_x}{\partial N} \right\rangle_N = 2\pi Q_x + \sum_{jklm} h_{jklm} \left(\frac{j+k}{2}\right) (2J_x)^{\frac{j+k}{2}-1} \left(2J_y\right)^{\frac{l+m}{2}} \lim_{N\to\infty} \frac{1}{N} \int_0^N dN' \; e^{2\pi i\left[(j-k)Q_x+(l-m)Q_y\right]N'}. \quad (2.54)$$

A closer look into the integral in Eq. 2.54 reveals that this integral in the limit where $N \to \infty$ is just a delta function reading $\delta\left((j-k)Q_x + (l-m)Q_y\right)$. As a reminder, the RDT approximation breaks down if Eq. 2.33 holds. Therefore, it can be shown that the argument in the delta function can only be zero if $j = k$ and $l = m$. Thus, this delta function effectively becomes two Kronecker deltas—δ_{jk} and δ_{lm}. Inserting this into Eq. 2.54 yields:

$$\lim_{N\to\infty} \left\langle \frac{\partial \phi_x}{\partial N} \right\rangle_N = 2\pi Q_x + \sum_{jklm} h_{jklm} \left(\frac{j+k}{2}\right) (2J_x)^{\frac{j+k}{2}-1} \left(2J_y\right)^{\frac{l+m}{2}} \delta_{jk}\delta_{lm}. \quad (2.55)$$

Reducing this expression further with the properties of Kronecker deltas reads:

$$\lim_{N\to\infty}\left\langle\frac{\partial\phi_x}{\partial N}\right\rangle_N = 2\pi Q_x + \sum_{jl} h_{jjll}\, j\,(2J_x)^{j-1}\left(2J_y\right)^l . \tag{2.56}$$

Equation 2.56 is stating that the constant detuning terms in the accelerators will be given by the terms where $j = k$ and $l = m$. As a consequence of Eq. 2.31, for this case the RDTs will be real numbers, i.e., $h_{jklm} \in \mathbb{R}$. Therefore, the constant detuning terms will come from even orders of $n = j + k + l + m$. It is worth remembering that this is a first approximation given that the assumption is that the dynamics are mainly governed by H_0. Higher order approximations would involve recursively solving Eqs. 2.49 and 2.50 as a Taylor expansion of the actions J_u [24].

As an example, Eq. 2.56 can be used to calculate the detuning due to horizontal quadrupole errors $n = 2$. For this, the calculation would only involve calculating h_{1100} from Eq. 2.31, the only surviving term. Therefore, the detuning in x due to quadrupole errors would read

$$\lim_{N\to\infty}\left\langle\frac{\partial\phi_x}{\partial N}\right\rangle_N = 2\pi Q_x + 2h_{1100} = 2\pi Q_x - \frac{1}{2}\sum_i L_i K_{1,i}\beta_{x,i} = 2\pi Q_x - \frac{1}{2}\sum_i L_i \frac{b_{1,i}}{\rho}\beta_{x,i}, \tag{2.57}$$

where the sum over i goes around all the quadrupole errors in the ring. Equation 2.57 gives a well-known result in accelerator physics [1].

Another example

2.7 Space Charge Tune Shift

Up to this point, the beam dynamics of high energy particle accelerators has been explained in terms of single-particle dynamics. Up until now, a couple of implicit assumptions have been made: (a) particles do not interact with each other; and (b) the LEGO® blocks composing the lattice have been idealized to create the fields but without supplying any electromagnetic boundary conditions. Nevertheless, in order to have a model closer to reality, the interaction between particles through the Coulomb force has to be taken into account. Furthermore, particles also interact with the electromagnetic properties of the lattice LEGO® blocks, ultimately, creating unwanted electromagnetic wake fields. This latter phenomenon opens another branch of accelerator physics that studies collective beam instabilities [25]. However, the scope of this thesis is only interested

in the first bullet point regarding direct particle-particle interactions through the Coulomb force—widely known as space charge physics. It is worth specifying that this restricts the analysis to a single bunch of particles.

As mentioned in Sec. 2.4, the Coulomb force will act as a detuning force on each individual particle. In order to explain this statement using a Hamiltonian formalism, the starting point needs to be the single-particle Hamiltonian that includes the Coulomb potential from the charge distribution in the bunch [26]. The expression for this system reads:

$$H(x, y, s) = H_0(x, y, s) + H_1(x, y, s) + \psi(x, y, \tilde{z}, s), \tag{2.58}$$

keeping in mind that x and y are interchangeable for their respective action-phase variables J_x, ϕ_x, J_y, ϕ_y. For a bunched beam, the variable $\tilde{z} = z - z_b$ is introduced in order to represent the longitudinal distance from the center of the bunch, always keeping in mind that the reference system moves with the bunch as described by a Frenet-Serret coordinate system. The center of the bunch with coordinates $(0, 0, z_b)$ is determined from the centroid of the longitudinal charge distribution. Additionally, the self-potential $\psi(x, y, \tilde{z}, s)$ is determined self-consistently from the 3D Poisson equation with a particle number density $n_b(x, y, \tilde{z}, s)$ reading:

$$\left(\frac{\partial}{\partial x} + \frac{\partial}{\partial y} + \frac{\partial}{\partial \tilde{z}}\right)\psi(x, y, \tilde{z}, s) = \frac{2\pi K_b}{N_b} n_b(x, y, \tilde{z}, s), \tag{2.59}$$

where K_b is a dimensionless parameter known as the self-field perveance defined as

$$K_b = \frac{2N_b e_b^2}{\gamma_L^3 m_b \beta_L^2 c^2}, \tag{2.60}$$

with N_b being the total number of particles in the bunch defined as $N_b = \int dx\, dy\, d\tilde{z}\, n_b(x, y, \tilde{z}, s)$, e_b is the charge of one beam particle, m_b is the rest mass of one beam particle, γ_L and β_L being the relativistic longitudinal factors of a beam with total energy $E_T = \gamma_L m_b c^2$, and c being the speed of light.

The solution to Eq. 2.59 can be found in any mathematical methods for physics book, see Refs. [27, 28]. The solution to this equation involves using Green's function and finding the convolution

with the particle number density $n_b(x, y, \tilde{z}, s) = n_b(\vec{r}, s)$. This reads:

$$\psi(x, y, \tilde{z}, s) = -\frac{2\pi K_b}{N_b} \int_{\mathbb{R}^3} d\vec{r}' \; \frac{n(\vec{r}, s)}{|\vec{r} - \vec{r}'|}. \tag{2.61}$$

CHAPTER 3

THE FNAL RECYCLER RING

The Fermilab Recycler Ring (RR) is one of the circular accelerators located in the Fermilab Accelerator Complex. It was originally designed to store and accumulate antiprotons that remained from a Tevatron event [29]. The recycling of antiprotons was deemed ineffective and was never operationally implemented [30]. Since 2011, the RR has been repurposed to act as a pre-injector to the Main Injector (MI) by storing and accumulating protons [14]. It is worth pointing out, that the MI and the RR share the same tunnel, which has a circumference of 3.319 km (2.062 mi).

The MI/RR complex is fed protons by the Proton Source, which by itself consists of the Pre-Accelerator, the Linear Accelerator (Linac), and the Booster. The Pre-Accelerator systems provide H^- ions to the Linac, where they are accelerated to an energy of 400 MeV. After this, the beam is injected into the Booster Ring. The Booster is a rapid-cycling synchrotron operating at a 15 Hz repetition rate. During this injection process, the H^- beam passes through a carbon stripping foil, and it incorporates to the circulating proton beam. The Booster ramps the energy up from 400 MeV to 8 GeV. This 8 GeV proton beam can either go to the Booster Neutrino Experiments or get injected into the Recycler Ring. Once in RR the beam has two possible destinations: 1) high energy neutrino experiments through MI or 2) Muon Campus. For the latter, proton beam gets rebunched from 53 MHz to 2.5 MHz and transported to Muon Campus. For high energy neutrino experiments, the proton beam gets slip-stacked, hence doubling the intensity that gets injected into Main Injector. Once in MI, the beam is accelerated to 120 GeV and sent to the NuMI (Neutrinos at the Main Injector) beam facility [13, 14, 30]. A description of the accelerator complex is shown in figure 3.1, including the experimental beamlines which feed neutrino, muon and fixed target experiments.

The work done for this thesis focuses on the Recycler Ring. The following chapter starts by giving a general description for the operation and physics of the Recycler Ring. The next sections introduce and motivate the compensation of third order resonances for high intensity operation.

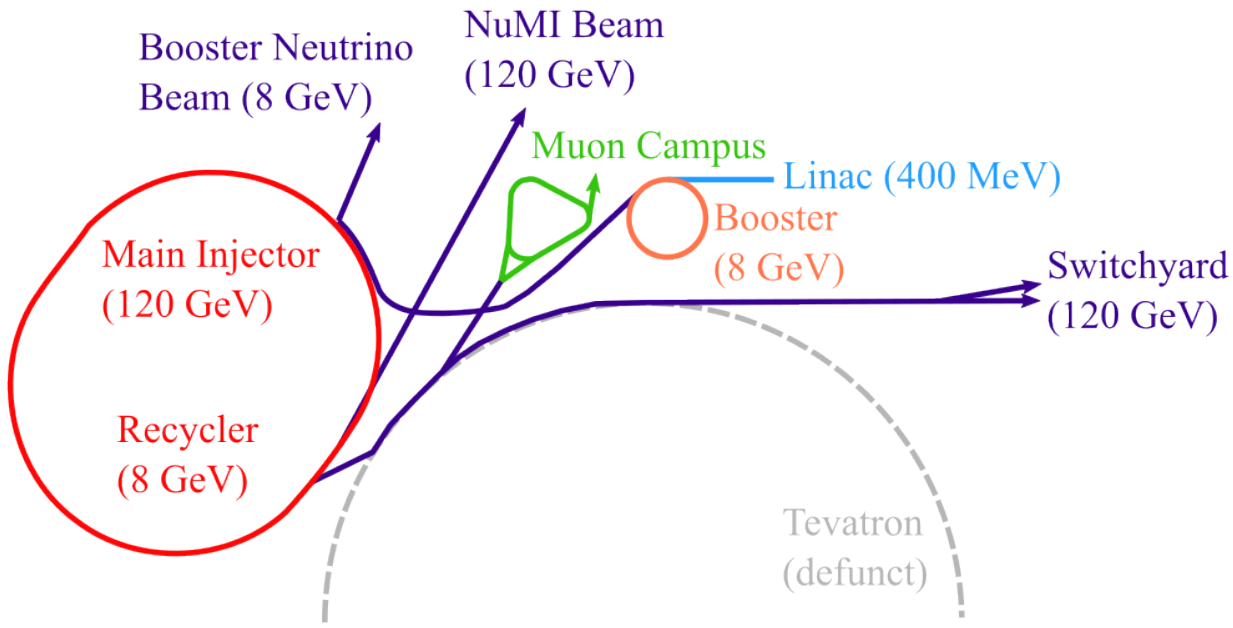

Figure 3.1 The past (Tevatron), present and future (PIP-II and LBNF) of the FNAL Accelerator Complex, taken from [3].

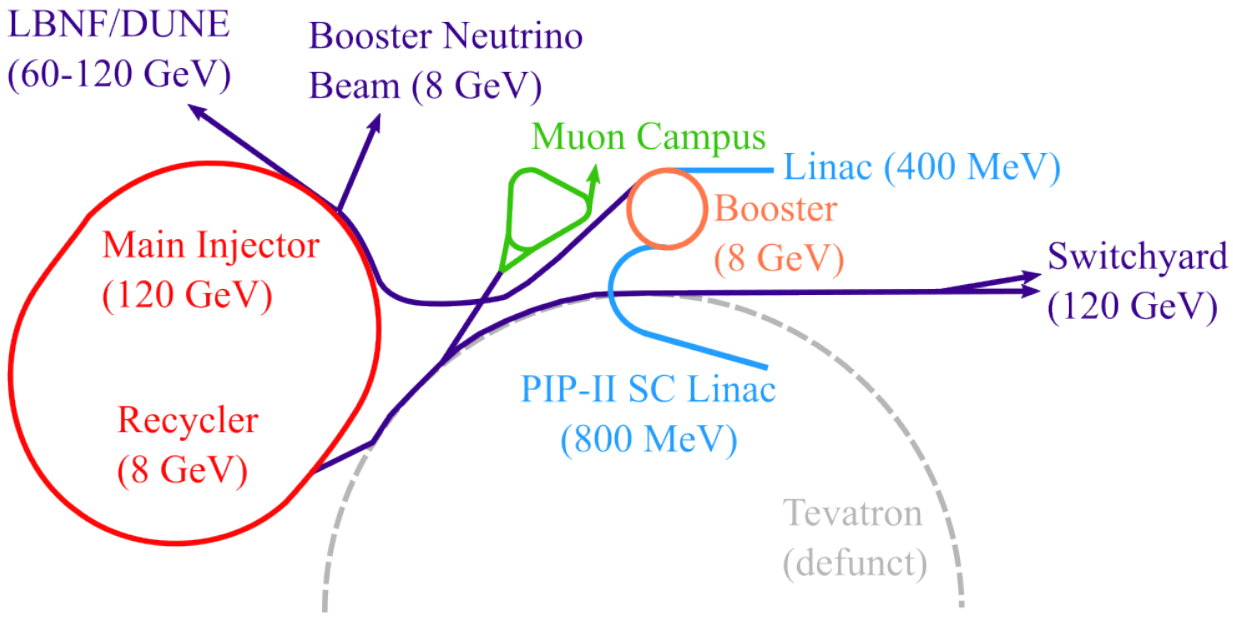

Figure 3.2 The past (Tevatron), present and future (PIP-II and LBNF) of the FNAL Accelerator Complex, taken from [3].

3.1 General Specifications

The RR is a permanent magnet storage ring operating at a fixed momentum of 8.835 GeV/c. [31] [32]

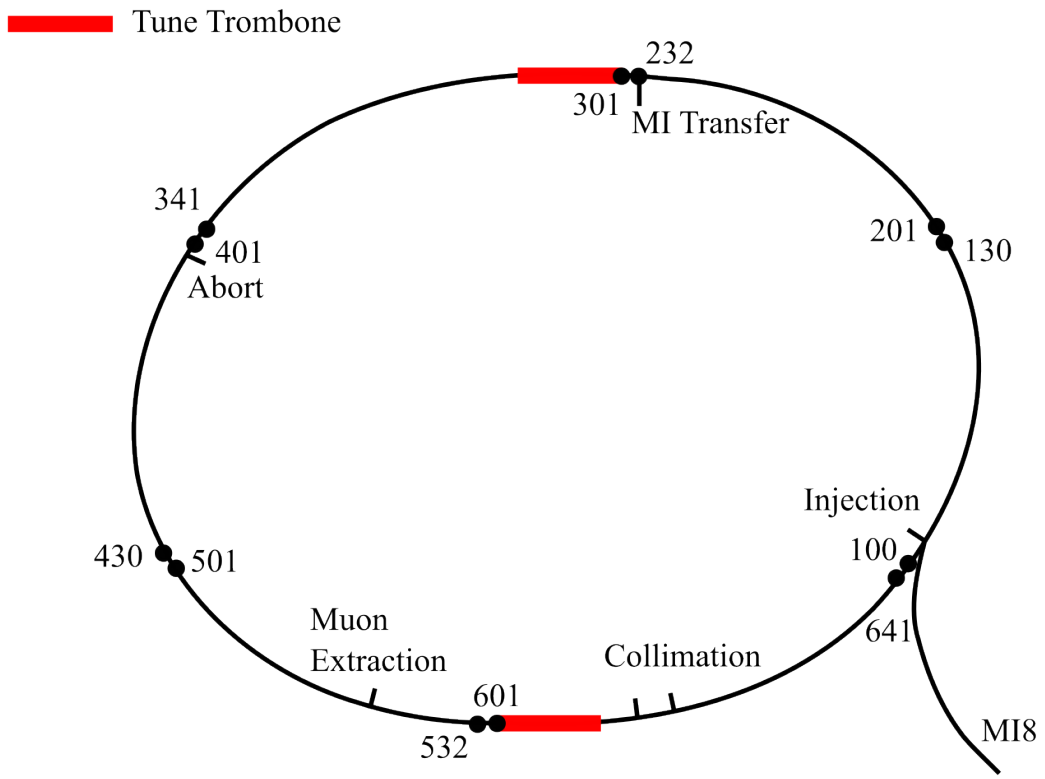

Figure 3.3 Schematic layout of the Recycler Ring and its corresponding sections. Original plot provided by R. Ainsworth, first published on Ref. [14].

Table 3.1 Typical Recycler Ring properties for beam sent to NuMI

Parameter	**Value**	**Unit**
Circumference	3319	m
Momentum	8.835	GeV/c
RF Frequency	52.8	MHz
RF Voltage	80	kV
Harmonic Number	588	
Synchrotron Tune	0.0028	
Slip Factor	-8.6×10^{-3}	
Superperiodicity	2	
Horizontal Tune	25.43	
Vertical Tune	24.445	
Horizontal Chromaticity	-6	
Vertical Chromaticity	-7	
95% Normalized Emittance	15	π mm mrad
95% Longitudinal Emittance	0.08	eV s
Intensity	5×10^{10}	ppb
	8×10^{10} (PIP-II)	ppb
MI Ramp Time	1.2	s
	1.133	s
	1.067	s
Booster Frequency	15	Hz
	20 (PIP-II)	Hz

3.2 Tune Diagram and Resonances

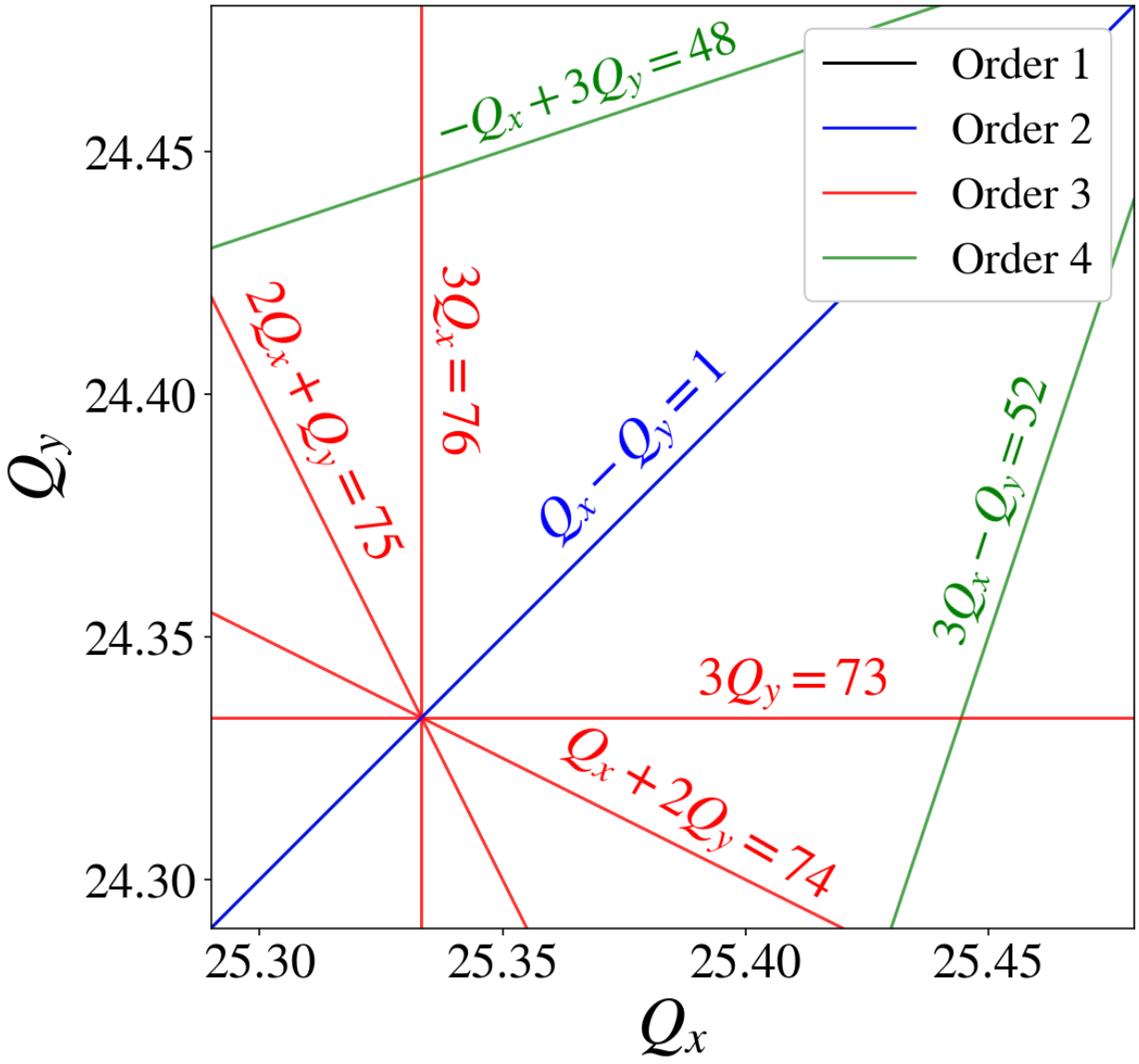

Figure 3.4 Portion of the tune diagram enclosing the operational tunes of the Recycler Ring.

3.3 High Intensity and Tune Footprint

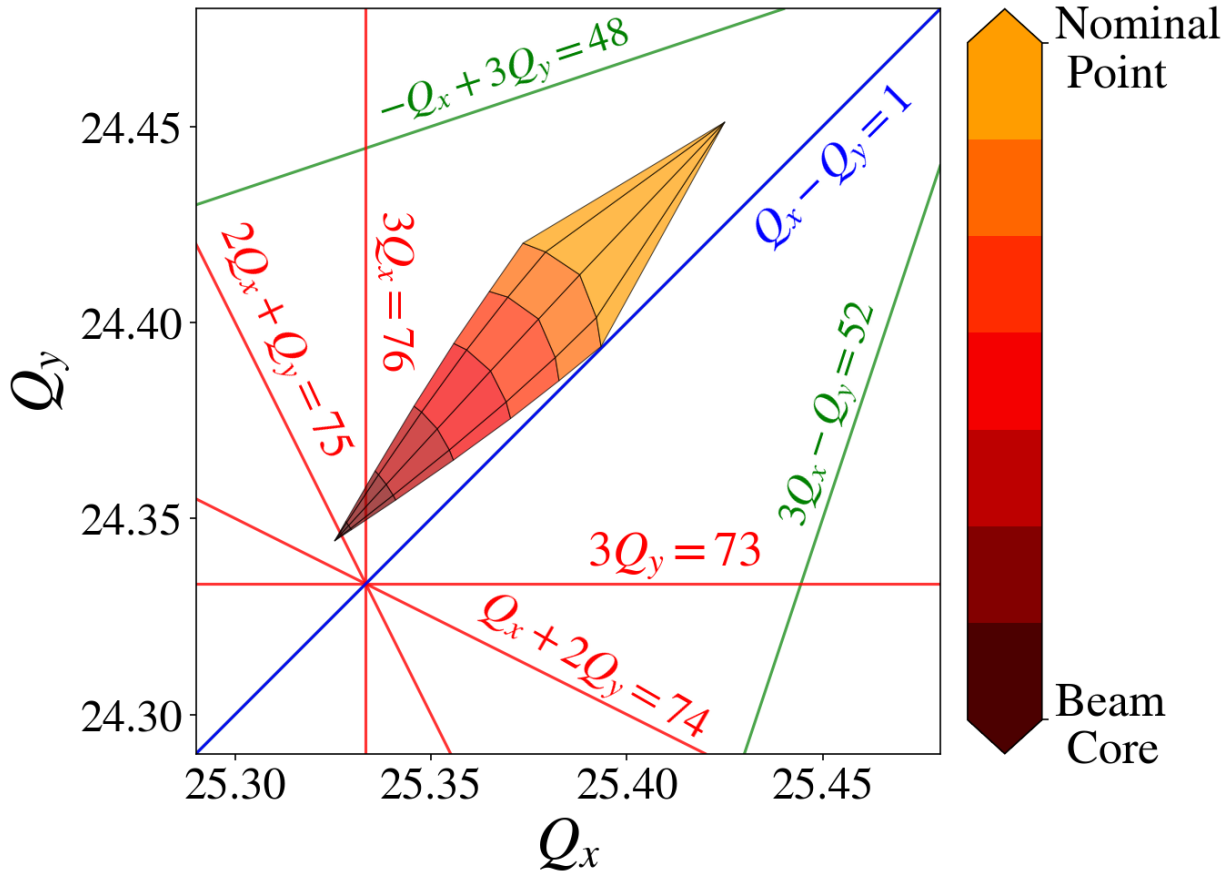

Figure 3.5 Approximate operational tune footprint at high intensities, i.e., 1e11 particles per bunch.

CHAPTER 4

COMPENSATION OF THIRD-ORDER RESONANCES AT LOW INTENSITIES

4.1 Global RDTs and Lattice Model

4.2 Measurement of Third Order RDTs

4.3 Compensation of RDTs

4.4 Optimization of Compensation Currents

4.5 Experimental Verification of Compensation

4.5.1 Dynamic Loss Map

4.5.2 Static Tune Scans

CHAPTER 5

RESONANCE COMPENSATION STUDIES AT THE CERN PROTON SYNCHROTRON BOOSTER

5.1 General specifications

5.2 Tune Diagram and Operation

5.3 Optimization Algorithms for Resonance Compensation

5.4 Experimental Verification of Compensation

CHAPTER 6

HIGH INTENSITY STUDIES

6.1 Global RDTs and Intensity-Dependent Effects

[33]

6.2 Space Charge Tune Shift

6.3 Measurement of Tune Shift

6.4 Static Tune Scans at Different Intensities

CHAPTER 7

CONCLUSIONS AND FUTURE WORK

[34] [35]

BIBLIOGRAPHY

[1] S Y Lee. *Accelerator Physics*. 3rd. WORLD SCIENTIFIC, 2011. DOI: 10.1142/8335. eprint: https://www.worldscientific.com/doi/pdf/10.1142/8335. URL: https://www.worldscientific.com/doi/abs/10.1142/8335.

[2] Lillian Hoddeson, Adrienne W. Kolb, and Catherine Westfall. *Fermilab: Physics, the Frontier, and Megascience*. University of Chicago Press, Dec. 2008. ISBN: 9780226346236. DOI: 10.7208/chicago/9780226346250.001.0001. URL: https://doi.org/10.7208/chicago/9780226346250.001.0001.

[3] David Griffiths. "Historical Introduction to the Elementary Particles". In: *Introduction to Elementary Particles*. John Wiley and Sons, Ltd, 1987. Chap. 1, pp. 11–53. ISBN: 9783527618460. DOI: https://doi.org/10.1002/9783527618460.ch1. eprint: https://onlinelibrary.wiley.com/doi/pdf/10.1002/9783527618460.ch1. URL: https://onlinelibrary.wiley.com/doi/abs/10.1002/9783527618460.ch1.

[4] Michigan State University. *Facility for Rare Isotope Beams at Michigan State University*. https://frib.msu.edu/index.php.

[5] SLAC National Accelerator Laboratory. *The Stanford Linear Accelerator Center at SLAC*. https://www.slac.stanford.edu/gen/grad/GradHandbook/slac.html.

[6] S. Holmes et al. "Accelerator physics at the Tevatron Collider: Introduction". In: *Accelerator physics at the Tevatron Collider*. Ed. by Valery Lebedev and Vladimir Shiltsev. 2014, pp. 1–28. DOI: 10.1007/978-1-4939-0885-1_1.

[7] CERN. *The Large Hadron Collider (LHC)*. https://home.cern/science/accelerators/large-hadron-collider.

[8] Ferdinand Willeke and J. Beebe-Wang. *Electron Ion Collider Conceptual Design Report 2021*. Tech. rep. BNL-221006-2021-FORE. Brookhaven National Laboratory, Feb. 2021. DOI: 10.2172/1765663. URL: https://www.osti.gov/biblio/1765663.

[9] Étienne Forest. *Beam Dynamics: A New Attitude and Framework*. Vol. 8. The Physics and Technology of Particle and Photon Beams. Amsterdam, The Netherlands: Hardwood Academic / CRC Press, 1998. ISBN: 978-90-5702-574-7.

[10] E Kako, P Pierini, and C.E. Reece. https://cerncourier.com/a/teslas-high-gradient-march/. Dec. 2020.

[11] Reidar Hahn. *Fermilab*. File: https://upload.wikimedia.org/wikipedia/commons/3/3f/Fermilab.jpg. 2003. URL: https://en.wikipedia.org/wiki/File:Fermilab.jpg.

[12] Swapan Chattopadhyay and Joseph David Lykken. *Fermilab at 50*. WORLD SCIENTIFIC, 2017. DOI: 10.1142/10637. eprint: https://www.worldscientific.com/doi/pdf/10.1142/10637. URL: https://www.worldscientific.com/doi/abs/10.1142/10637.

[13] P. Adamson et al. "The NuMI neutrino beam". In: *Nuclear Instruments and Methods in Physics Research Section A: Accelerators, Spectrometers, Detectors and Associated Equipment* 806 (2016), pp. 279–306. ISSN: 0168-9002. DOI: https://doi.org/10.1016/j.nima.2015.08.063. URL: https://www.sciencedirect.com/science/article/pii/S016890021501027X.

[14] R. Ainsworth et al. "High intensity operation using proton stacking in the Fermilab Recycler to deliver 700 kW of 120 GeV proton beam". In: *Phys. Rev. Accel. Beams* 23 (12 Dec. 2020), p. 121002. DOI: 10.1103/PhysRevAccelBeams.23.121002. URL: https://link.aps.org/doi/10.1103/PhysRevAccelBeams.23.121002.

[15] Andrzej Wolski. *Beam Dynamics in High Energy Particle Accelerators*. 2nd. WORLD SCIENTIFIC, 2023. DOI: 10.1142/13333. eprint: https://www.worldscientific.com/doi/pdf/10.1142/13333. URL: https://www.worldscientific.com/doi/abs/10.1142/13333.

[16] Helmut Wiedemann. *Resonances*. Cham: Springer International Publishing, 2015, pp. 539–564. ISBN: 978-3-319-18317-6. DOI: 10.1007/978-3-319-18317-6_16. URL: https://doi.org/10.1007/978-3-319-18317-6_16.

[17] T. Satogata. *Lecture Notes on Poisson Brackets and Lie Operators*. https://toddsatogata.net/2011-USPAS/lieAlgebras.pdf. Jan. 2008.

[18] P. Urschutz. "Measurement and Compensation of Betatron Resonances at the CERN PS Booster Synchrotron". PhD thesis. Vienna, Austria, 2004.

[19] R. Tomas Garcia. "Direct Measurement of Resonance Driving Terms in the Super Proton Synchrotron (SPS) of CERN using Beam Position Monitors". PhD thesis. Valencia, Spain, Jan. 2003.

[20] Wolfram Research Inc. *Mathematica Online, Version 13.3*. URL: https://www.wolfram.com/mathematica.

[21] Rüdiger Achilles and Andrea Bonfiglioli. "The early proofs of the theorem of Campbell, Baker, Hausdorff, and Dynkin". In: *Archive for History of Exact Sciences* 66.3 (May 2012), pp. 295–358. DOI: 10.1007/s00407-012-0095-8. URL: https://doi.org/10.1007/s00407-012-0095-8.

[22] R Bartolini and F Schmidt. "Normal form via tracking or beam data". In: *Part. Accel.* 59 (1998), pp. 93–106. URL: https://cds.cern.ch/record/333077.

[23] *MAD-X: Methodical Accelerator Design*. http://madx.web.cern.ch/madx.

[24] Kouichi Soutome and Hitoshi Tanaka. "Higher-order formulas of amplitude-dependent tune shift caused by a sextupole magnetic field distribution". In: *Phys. Rev. Accel. Beams* 20 (6 June 2017), p. 064001. DOI: 10.1103/PhysRevAccelBeams.20.064001. URL: https://link.aps.org/doi/10.1103/PhysRevAccelBeams.20.064001.

[25] A. W. Chao. *Physics of collective beam instabilities in high-energy accelerators*. 1993. ISBN: 978-0-471-55184-3.

[26] Ronald C Davidson and Hong Qin. *Physics of Intense Charged Particle Beams in High Energy Accelerators*. IMPERIAL COLLEGE PRESS CO-PUBLISHED WITH WORLD SCIENTIFIC PUBLISHING CO, 2001. DOI: 10.1142/p250. eprint: https://www.worldscientific.com/doi/pdf/10.1142/p250. URL: https://www.worldscientific.com/doi/abs/10.1142/p250.

[27] George B. Arfken, Hans J. Weber, and Frank E. Harris. "Chapter 10 - Green's Functions". In: *Mathematical Methods for Physicists (Seventh Edition)*. Ed. by George B. Arfken, Hans J. Weber, and Frank E. Harris. Seventh Edition. Boston: Academic Press, 2013, pp. 447–467. ISBN: 978-0-12-384654-9. DOI: https://doi.org/10.1016/B978-0-12-384654-9.00010-4.

[28] Gabriel Tellez Acosta. *Metodos Matemeticos*. Ediciones Uniandes, 2022. ISBN: 9789587981827.

[29] G. Jackson. *The Fermilab recycler ring technical design report. Revision 1.2*. Tech. rep. FNAL-TM-1991ON: DE97051388; BR: KAHEP. Fermilab, Nov. 1996. DOI: 10.2172/16029. URL: https://www.osti.gov/biblio/16029.

[30] S. Nagaitsev. *Fermilab Antiproton source, Recycler ring and Main Injector*. Tech. rep. FERMILAB-FN-0957-AD. Fermilab, Mar. 2013. DOI: 10.2172/1127965. URL: https://www.osti.gov/biblio/1127965.

[31] M. Ball et al. *The PIP-II Conceptual Design Report*. Tech. rep. FERMILAB-TM-2649-AD-APC1516858. Fermilab, Mar. 2017. DOI: 10.2172/1346823. URL: https://www.osti.gov/biblio/1346823.

[32] R. Ainsworth et al. "High intensity space charge effects on slip stacked beam in the Fermilab Recycler". In: *Phys. Rev. Accel. Beams* 22 (2 Feb. 2019), p. 020404. DOI: 10.1103/PhysRevAccelBeams.22.020404. URL: https://link.aps.org/doi/10.1103/PhysRevAccelBeams.22.020404.

[33] N. Chelidze, R. Ainsworth, and K.J. Hazelwood. "The Effect of the Main Injector Ramp on the Recycler". In: *Proc. 5th Int. Particle Accel. Conf. (NAPAC'22)* (Albuquerque, NM, USA). International Particle Accelerator Conference 5. JACoW Publishing, Geneva, Switzerland, Oct. 2022, MOPA19, pp. 90–92. ISBN: 978-3-95450-232-5. DOI: 10.18429/

JACoW-NAPAC2022-MOPA19. URL: https://jacow.org/napac2022/papers/mopa19.pdf.

[34] C.E. Gonzalez-Ortiz, R. Ainsworth, and P.N. Ostroumov. "Third-Order Resonance Compensation at the FNAL Recycler Ring". In: *Proc. IPAC'22* (Bangkok, Thailand). International Particle Accelerator Conference 13. JACoW Publishing, Geneva, Switzerland, July 2022, MOPOST050, pp. 195–198. ISBN: 978-3-95450-227-1. DOI: 10.18429/JACoW-IPAC2022-MOPOST050. URL: https://jacow.org/ipac2022/papers/mopost050.pdf.

[35] C.E. Gonzalez-Ortiz, R. Ainsworth, and P.N. Ostroumov. "Simultaneous Compensation of Third-Order Resonances at the FNAL Recycler Ring". In: *Proc. IPAC'23* (Venezia). IPAC'23 - 14th International Particle Accelerator Conference 14. JACoW Publishing, Geneva, Switzerland, May 2023, pp. 3328–3331. ISBN: 978-3-95450-231-8. DOI: doi:10.18429/jacow-ipac2023-wepl112. URL: https://www.ipac23.org/preproc/pdf/WEPL112.pdf.

APPENDIX A

LIE ALGEBRA METHODS FOR ACCELERATOR PHYSICS IN 2D USING MATHEMATICA

Lie Algebra methods for Accelerator Physics in 2D

1. Poisson Brackets, Lie Operator and Exponential Lie Operators

```
In[•]:= PoissonBracket[f_, g_, q_Symbol, p_Symbol] :=
         Simplify[D[f, q] * D[g, p] - D[f, p] * D[g, q]]

In[•]:= PoissonBracket[f[x, p], g[x, p], x, p]
Out[•]=
        g^(0,1)[x, p] f^(1,0)[x, p] - f^(0,1)[x, p] g^(1,0)[x, p]

In[•]:= LieOperator[f_] := Function[g, PoissonBracket[f, g, x, p]]

In[•]:= LieOperator[f[x, p]][g[x, p]]
Out[•]=
        g^(0,1)[x, p] f^(1,0)[x, p] - f^(0,1)[x, p] g^(1,0)[x, p]

In[•]:= ExpOperator[oprtr_, n_ : 10] :=
         Function[f, Fold[f + oprtr[#1] / #2 &, f, Reverse@Range[n]]]

In[•]:= DiffOperator := Function[f, D[f, x]]

In[•]:= Simplify[ExpOperator[DiffOperator, 4][f[x]]]
Out[•]=
        f[x] + f'[x] + f''[x]/2 + 1/6 f^(3)[x] + 1/24 f^(4)[x]

In[•]:= ExpOperator[LieOperator[f[x, p]], 1][g[x, p]]
Out[•]=
        g[x, p] + g^(0,1)[x, p] f^(1,0)[x, p] - f^(0,1)[x, p] g^(1,0)[x, p]
```

2. Lie Methods for common accelerator elements

```
In[•]:= Drift[L_, n_ : 10] := Function[g, ExpOperator[LieOperator[-0.5 * L * p^2], n][g]]
```

```
In[•]:= Map[Drift[L], {x, p}]
```

Out[•]=

$$\{0. + 1.\ L\ p + x,\ 0. + p\}$$

```
In[•]:= ThinQuad[kL_, n_ : 10] := Function[g, ExpOperator[LieOperator[-0.5 * kL * x^2], n][g]]

In[•]:= Map[ThinQuad[kL], {x, p}]
```

Out[•]=

$$\{0. + x,\ 0. + p - 1.\ kL\ x\}$$

```
In[•]:= ThinKick[k_, m_, n_ : 10 ] := Function[g, ExpOperator[LieOperator[k * x^m], n][g]]

In[•]:= Map[ThinKick[λ, n], {x, p}]
```

Out[•]=

$$\left\{x,\ p + n\ x^{-1+n}\ \lambda\right\}$$

```
In[•]:= ThickQuad[k_, L_, n_ : 10] := Function[g,
          ExpOperator[LieOperator[-Sign[k] * 0.5 * L * (k * x^2 + Sign[k] * p^2)], n][g]]

In[•]:= Collect[Assuming[k < 0, ThickQuad[k, L, 3][x]], {x, p}]
```

Out[•]=

$$L\left(1. + 0.166667\ k\ L^2\right)\ p + \left(1 + 0.5\ k\ L^2\right)\ x$$

```
In[•]:= Collect[Assuming[k < 0, ThickQuad[k, L, 3][p]], {x, p}]
```

Out[•]=

$$\left(1 + 0.5\ k\ L^2\right)\ p + \left(1.\ k\ L + 0.166667\ k^2\ L^3\right)\ x$$

```
In[•]:= ThickFQuad[k_, L_, n_ : 10] :=
         Function[g, ExpOperator[LieOperator[-0.5 * L * (k * x^2 + p^2)], n][g]]

In[•]:= Collect[ThickFQuad[k, L, 10][p], {x, p}]
```

Out[•]=

$$\left(1 - 0.5\ k\ L^2 - 2.75573 \times 10^{-7}\ k^2\ L^3\ \left(-151\,200.\ L + 5040.\ k\ L^3 - 90.\ k^2\ L^5 + 1.\ k^3\ L^7\right)\right)\ p + \left(-1.\ k\ L - 2.75573 \times 10^{-6}\ k^2\ L^3\ \left(-60\,480. + 3024.\ k\ L^2 - 72.\ k^2\ L^4 + 1.\ k^3\ L^6\right)\right)\ x$$

```
In[•]:= ThickDQuad[k_, L_, n_ : 10] :=
         Function[g, ExpOperator[LieOperator[0.5 * L * (k * x^2 - p^2)], n][g]]

In[•]:= Collect[ThickDQuad[k, L, 6][p], {x, p}]
```

Out[•]=

$$\left(1 + 0.5\ k\ L^2 + 0.0416667\ k^2\ L^4 + 0.00138889\ k^3\ L^6\right)\ p + \left(1.\ k\ L + 0.166667\ k^2\ L^3 + 0.00833333\ k^3\ L^5\right)\ x$$

```
In[•]:= Collect[ExpOperator[LieOperator[(0.5 * p^2 + k * x^2) * s]][x], {x, p}]
```

Out[•]=

$$\frac{1}{3}\ p\ s\ \left(-3. + 1.\ k\ s^2 - 0.1\ k^2\ s^4 + 0.0047619\ k^3\ s^6 - 0.000132275\ k^4\ s^8\right) + \left(1 + \frac{1}{3}\ k\ s^2\ \left(-3. + 0.5\ k\ s^2 - 0.0333333\ k^2\ s^4 + 0.00119048\ k^3\ s^6 - 0.000026455\ k^4\ s^8\right)\right)\ x$$

```
In[•]:= Collect[ExpOperator[LieOperator[-(0.5 * p^2 + k * x^3 / 6) * s], 3][x], {x, p}]
```

Out[•]=

$$1.\, p\, s + \left(1 - 0.166667\, k\, p\, s^3\right) x - 0.25\, k\, s^2\, x^2$$

3. Concatenating elements by composition of maps

```
In[•]:= Map[Composition[Drift[L], Drift[L]], {x, p}]
```

Out[•]=

$$\{0. + 2.\, L\, p + x,\ 0. + p\}$$

FODO Lattice

```
In[•]:= Collect[Simplify[Composition[ThinQuad[-1 / (2 f)],
    Drift[L], ThinQuad[1 / f], Drift[L], ThinQuad[-1 / (2 f)]][x]], {x, p}]
```

Out[•]=

$$0. + \left(2.\, L - \frac{1.\, L^2}{f}\right) p + \left(1 - \frac{0.5\, L^2}{f^2}\right) x$$

```
In[•]:= Collect[Simplify[Composition[ThinQuad[-1 / (2 f)],
    Drift[L], ThinQuad[1 / f], Drift[L], ThinQuad[-1 / (2 f)]][p]], {x, p}]
```

Out[•]=

$$0. + \left(1 - \frac{0.5\, L^2}{f^2}\right) p + \left(-\frac{0.5\, L}{f^2} - \frac{0.25\, L^2}{f^3}\right) x$$

APPENDIX B

LIE ALGEBRA METHODS FOR ACCELERATOR PHYSICS IN 4D USING MATHEMATICA

Lie Algebra methods for Accelerator Physics in 4D

Chapter 1. Poisson Brackets and Lie Algebra in 4D

```
In[•]:= PoissonBracket[a_, b_, q_List, p_List] := Block[{pk, n}, n = Length[q];
          If[n == Length[p],
           pk = Simplify[Sum[D[a, q[[j]]] × D[b, p[[j]]] - D[b, q[[j]]] × D[a, p[[j]]], {j, 1, n}]],
           Print["Incompatible lengths"]]]
```

```
In[•]:= PoissonBracket[f[x, px, y, py], g[x, px, y, py], {x, y}, {px, py}]
```

```
Out[•]=
g^(0,0,0,1)[x, px, y, py] f^(0,0,1,0)[x, px, y, py] -
 f^(0,0,0,1)[x, px, y, py] g^(0,0,1,0)[x, px, y, py] +
 g^(0,1,0,0)[x, px, y, py] f^(1,0,0,0)[x, px, y, py] -
 f^(0,1,0,0)[x, px, y, py] g^(1,0,0,0)[x, px, y, py]
```

```
In[•]:= LieOperator[f_] := Function[g, PoissonBracket[f, g, {x, y}, {px, py}]]
```

```
In[•]:= LieOperator[f[x, y, px, py]][g[x, y, px, py]]
```

```
Out[•]=
g^(0,0,0,1)[x, y, px, py] f^(0,1,0,0)[x, y, px, py] -
 f^(0,0,0,1)[x, y, px, py] g^(0,1,0,0)[x, y, px, py] +
 g^(0,0,1,0)[x, y, px, py] f^(1,0,0,0)[x, y, px, py] -
 f^(0,0,1,0)[x, y, px, py] g^(1,0,0,0)[x, y, px, py]
```

```
In[•]:= ExpOperator[oprtr_, n_ : 10] :=
         Function[f, Fold[f + oprtr[#1] / #2 &, f, Reverse@Range[n]]]
```

```
In[•]:= Simplify[ExpOperator[LieOperator[f[x, y, px, py]], 1][g[x, y, px, py]]]
```

```
Out[•]=
g[x, y, px, py] + g^(0,0,0,1)[x, y, px, py] f^(0,1,0,0)[x, y, px, py] -
 f^(0,0,0,1)[x, y, px, py] g^(0,1,0,0)[x, y, px, py] +
 g^(0,0,1,0)[x, y, px, py] f^(1,0,0,0)[x, y, px, py] -
 f^(0,0,1,0)[x, y, px, py] g^(1,0,0,0)[x, y, px, py]
```

In[•]:=
```
Simplify[ExpOperator[LieOperator[f[x, y, px, py]], 2][g[x, y, px, py]]]
```

Out[•]=

$$
\begin{aligned}
&g[x, y, px, py] + \frac{1}{2}\Big(f^{(0,1,0,0)}[x, y, px, py]\\
&\quad\Big(g^{(0,0,0,2)}[x, y, px, py]\, f^{(0,1,0,0)}[x, y, px, py] - f^{(0,0,0,2)}[x, y, px, py]\\
&\qquad g^{(0,1,0,0)}[x, y, px, py] + g^{(0,0,0,1)}[x, y, px, py]\Big(2 + f^{(0,1,0,1)}[x, y, px, py]\Big) -\\
&\qquad f^{(0,0,0,1)}[x, y, px, py]\, g^{(0,1,0,1)}[x, y, px, py] + g^{(0,0,1,1)}[x, y, px, py]\\
&\qquad f^{(1,0,0,0)}[x, y, px, py] - f^{(0,0,1,1)}[x, y, px, py]\, g^{(1,0,0,0)}[x, y, px, py] +\\
&\qquad g^{(0,0,1,0)}[x, y, px, py]\, f^{(1,0,0,1)}[x, y, px, py] -\\
&\qquad f^{(0,0,1,0)}[x, y, px, py]\, g^{(1,0,0,1)}[x, y, px, py]\Big) +\\
&\quad f^{(1,0,0,0)}[x, y, px, py]\Big(g^{(0,0,1,1)}[x, y, px, py]\, f^{(0,1,0,0)}[x, y, px, py] -\\
&\qquad f^{(0,0,1,1)}[x, y, px, py]\, g^{(0,1,0,0)}[x, y, px, py] +\\
&\qquad g^{(0,0,0,1)}[x, y, px, py]\, f^{(0,1,1,0)}[x, y, px, py] - f^{(0,0,0,1)}[x, y, px, py]\\
&\qquad g^{(0,1,1,0)}[x, y, px, py] + g^{(0,0,2,0)}[x, y, px, py]\, f^{(1,0,0,0)}[x, y, px, py] -\\
&\qquad f^{(0,0,2,0)}[x, y, px, py]\, g^{(1,0,0,0)}[x, y, px, py] + g^{(0,0,1,0)}[x, y, px, py]\\
&\qquad \Big(2 + f^{(1,0,1,0)}[x, y, px, py]\Big) - f^{(0,0,1,0)}[x, y, px, py]\, g^{(1,0,1,0)}[x, y, px, py]\Big) +\\
&\quad f^{(0,0,0,1)}[x, y, px, py]\Big(g^{(0,1,0,0)}[x, y, px, py]\Big(-2 + f^{(0,1,0,1)}[x, y, px, py]\Big) -\\
&\qquad f^{(0,1,0,0)}[x, y, px, py]\, g^{(0,1,0,1)}[x, y, px, py] -\\
&\qquad g^{(0,0,0,1)}[x, y, px, py]\, f^{(0,2,0,0)}[x, y, px, py] + f^{(0,0,0,1)}[x, y, px, py]\\
&\qquad g^{(0,2,0,0)}[x, y, px, py] - g^{(0,1,1,0)}[x, y, px, py]\, f^{(1,0,0,0)}[x, y, px, py] +\\
&\qquad f^{(0,1,1,0)}[x, y, px, py]\, g^{(1,0,0,0)}[x, y, px, py] - g^{(0,0,1,0)}[x, y, px, py]\\
&\qquad f^{(1,1,0,0)}[x, y, px, py] + f^{(0,0,1,0)}[x, y, px, py]\, g^{(1,1,0,0)}[x, y, px, py]\Big) +\\
&\quad f^{(0,0,1,0)}[x, y, px, py]\Big(g^{(0,1,0,0)}[x, y, px, py]\, f^{(1,0,0,1)}[x, y, px, py] -\\
&\qquad f^{(0,1,0,0)}[x, y, px, py]\, g^{(1,0,0,1)}[x, y, px, py] +\\
&\qquad g^{(1,0,0,0)}[x, y, px, py]\Big(-2 + f^{(1,0,1,0)}[x, y, px, py]\Big) - f^{(1,0,0,0)}[x, y, px, py]\\
&\qquad g^{(1,0,1,0)}[x, y, px, py] - g^{(0,0,0,1)}[x, y, px, py]\, f^{(1,1,0,0)}[x, y, px, py] +\\
&\qquad f^{(0,0,0,1)}[x, y, px, py]\, g^{(1,1,0,0)}[x, y, px, py] - g^{(0,0,1,0)}[x, y, px, py]\\
&\qquad f^{(2,0,0,0)}[x, y, px, py] + f^{(0,0,1,0)}[x, y, px, py]\, g^{(2,0,0,0)}[x, y, px, py]\Big)\Big)
\end{aligned}
$$

In[•]:=
```
ExpLieOperator[f_, n_ : 10] := Function[g, ExpOperator[LieOperator[f], n][g]]
```

In[•]:=
```
ExpLieOperator[f[x, y, px, py], 1][g[x, y, px, py]]
```

Out[•]=

$$
\begin{aligned}
&g[x, y, px, py] + g^{(0,0,0,1)}[x, y, px, py]\, f^{(0,1,0,0)}[x, y, px, py] -\\
&\quad f^{(0,0,0,1)}[x, y, px, py]\, g^{(0,1,0,0)}[x, y, px, py] +\\
&\quad g^{(0,0,1,0)}[x, y, px, py]\, f^{(1,0,0,0)}[x, y, px, py] -\\
&\quad f^{(0,0,1,0)}[x, y, px, py]\, g^{(1,0,0,0)}[x, y, px, py]
\end{aligned}
$$

Chapter 2. Common Accelerator Elements

In[•]:=
```
Drift[L_, n_ : 10] := Function[g, ExpLieOperator[-0.5 * L * px^2 - 0.5 * L * py^2][g]]
```

```
In[•]:= Simplify[Map[Drift[L], {x, y, px, py}]]
```

Out[•]=

$$\{0. + 1.\ L\ px + x,\ 0. + 1.\ L\ py + y,\ 0. + px,\ 0. + py\}$$

```
In[•]:= ThinQuad[kL_, n_ : 10] := Function[g, ExpLieOperator[-0.5 * kL * x^2 + 0.5 * kL * y^2][g]]
```

```
In[•]:= Simplify[Map[ThinQuad[-1 / f], {x, y, px, py}]]
```

Out[•]=

$$\left\{0. + x,\ 0. + y,\ 0. + px + \frac{1.\ x}{f},\ 0. + py - \frac{1.\ y}{f}\right\}$$

```
In[•]:= Simplify[Map[ThinQuad[k], {x, y, px, py}]]
```

Out[•]=

$$\{0. + x,\ 0. + y,\ 0. + px - 1.\ k\ x,\ 0. + py + 1.\ k\ y\}$$

```
In[•]:= ThinSextupole[s_, n_ : 10] :=
         Function[g, ExpLieOperator[(1 / 3) * s * (x^3 - 3 * x * y^2), n][g]]
```

```
In[•]:= Map[ThinSextupole[s], {x, y, px, py}]
```

Out[•]=

$$\left\{x,\ y,\ px + s\ \left(x^2 - y^2\right),\ py - 2\ s\ x\ y\right\}$$

```
In[•]:= GetNormalHamiltonian[kn_, n_] := (1 / (1 + n)) * ComplexExpand[Re[kn * (x + I * y)^(n + 1)]]
```

```
In[•]:= Expand[GetNormalHamiltonian[k, 2]]
```

Out[•]=

$$\frac{k\ x^3}{3} - k\ x\ y^2$$

```
In[•]:= GetSkewHamiltonian[k_, n_] := (1 / (1 + n)) * ComplexExpand[Re[I * k * (x + I * y)^(n + 1)]]
```

```
In[•]:= Expand[GetSkewHamiltonian[k, 2]]
```

Out[•]=

$$-k\ x^2\ y + \frac{k\ y^3}{3}$$

```
In[•]:= ThinNormalMultipole[ki_, i_, n_ : 10] :=
         Function[g, ExpLieOperator[GetNormalHamiltonian[ki, i], n][g]]
```

```
In[•]:= Map[ThinNormalMultipole[k, 2], {x, y, px, py}]
```

Out[•]=

$$\left\{x,\ y,\ px + k\ \left(x^2 - y^2\right),\ py - 2\ k\ x\ y\right\}$$

```
In[•]:= ThinSkewMultipole[ki_, i_, n_ : 10] :=
         Function[g, ExpLieOperator[GetSkewHamiltonian[ki, i], n][g]]
```

```
In[•]:= Map[ThinSkewMultipole[k2s, 2], {x, y, px, py}]
```

Out[•]=

$$\left\{x,\ y,\ px - 2\ k2s\ x\ y,\ py + k2s\ \left(-x^2 + y^2\right)\right\}$$

```
In[•]:=
```

Hamiltonians of some machine elements (3D)

In general for multipole n:

$$H_n = \frac{1}{1+n}\mathcal{R}e\left[(k_n + \mathrm{i}k_n^{(s)})(x+\mathrm{i}y)^{n+1}\right] + \frac{p_x^2 + p_y^2}{2(1+\delta)}$$

We get for some important types (normal components k_n only

In[ ]:=

dipole: $H = -\frac{-x\delta}{\rho} + \frac{x^2}{2\rho^2} + \frac{p_x^2 + p_y^2}{2(1+\delta)}$

quadrupole: $H = \frac{1}{2}k_1(x^2 - y^2) + \frac{p_x^2 + p_y^2}{2(1+\delta)}$

sextupole: $H = \frac{1}{3}k_2(x^3 - 3xy^2) + \frac{p_x^2 + p_y^2}{2(1+\delta)}$

Such a field (force) we need for focusing

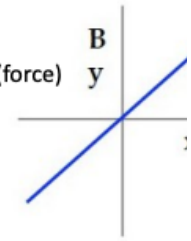

Out[ ]=

Hamiltonians of some machine elements (3D)

In general for multipole n:

$$H_n = \frac{1}{1+n}\mathcal{R}e\left[(k_n + \mathrm{i}k_n^{(s)})(x+\mathrm{i}y)^{n+1}\right] + \frac{p_x^2 + p_y^2}{2(1+\delta)}$$

We get for some important types (normal components k_n onl

dipole: $H = -\frac{-x\delta}{\rho} + \frac{x^2}{2\rho^2} + \frac{p_x^2 + p_y^2}{2(1+\delta)}$

quadrupole: $H = \frac{1}{2}k_1(x^2 - y^2) + \frac{p_x^2 + p_y^2}{2(1+\delta)}$

sextupole: $H = \frac{1}{3}k_2(x^3 - 3xy^2) + \frac{p_x^2 + p_y^2}{2(1+\delta)}$

Such a field (force) we need for focusing

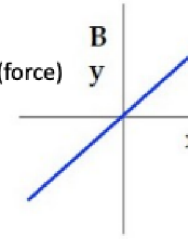

Chapter 3. Multiple elements and Map Composition

In[ ]:=
```
Map[Composition[Drift[L], Drift[L]], {x, y, px, py}]
```

Out[ ]=
```
{0. + 2. L px + x, 0. + 2. L py + y, 0. + px, 0. + py}
```

In[ ]:=

FODO Lattice

In[ ]:=
```
FODO[L_, K_, n_ : 10] := Function[g, Composition[ThinQuad[-0.5 * K],
    Drift[L], ThinQuad[K], Drift[L], ThinQuad[-0.5 * K]][g]]
```

In[ ]:=
```
Collect[Simplify[FODO[L, -1 / f][x]], {x, y, px, py}]
```

Out[ ]=
$$0. + \left(2.\,L + \frac{1.\,L^2}{f}\right) px + \left(1 - \frac{0.5\,L^2}{f^2}\right) x$$

In[•]:=
```
Collect[Simplify[FODO[L, -1 / f][y]], {x, y, px, py}]
```

Out[•]=

$$0. + \left(2.\, L - \frac{1.\, L^2}{f}\right) py + \left(1 - \frac{0.5\, L^2}{f^2}\right) y$$

In[•]:=
```
Collect[Simplify[FODO[L, -1 / f][px]], {x, y, px, py}]
```

Out[•]=

$$0. + \left(1 - \frac{0.5\, L^2}{f^2}\right) px + \left(-\frac{0.5\, L}{f^2} + \frac{0.25\, L^2}{f^3}\right) x$$

In[•]:=
```
Collect[Simplify[FODO[L, -1 / f][py]], {x, y, px, py}]
```

Out[•]=

$$0. + \left(1 - \frac{0.5\, L^2}{f^2}\right) py + \left(-\frac{0.5\, L}{f^2} - \frac{0.25\, L^2}{f^3}\right) y$$